Journal of Chromatography A 1731 (2024) 465212

Contents lists available at ScienceDirect

Journal of Chromatography A

journal homepage: www.elsevier.com/locate/chroma

Integrated system for temperature-controlled fast protein liquid chromatography. IV. Continuous 'one-column' 'low-salt' hydrophobic interaction chromatography

Alexander Brean [a,1], Tim W. Overton [a,b], Daniel G. Bracewell [c], Matthias Franzreb [d], Owen R. T. Thomas [a,*]

[a] School of Chemical Engineering, College of Engineering and Physica1, University of Birmingham, Edgbaston, Birmingham B15 2TT, England, UK
[b] Institute for Microbiology and Infection, University of Birmingham, Edgbaston, Birmingham B15 2TT, UK
[c] Department of Biochemical Engineering, University College London, London WC1E 6BT, UK
[d] Institute of Functional Interfaces, Karlsruhe Institute of Technology, Hermann-von-Helmholtz-Platz 1, 76344 Eggenstein-Leopoldshafen, Germany

ARTICLE INFO

Keywords:
Bioseparation
Bovine serum albumin, BSA
Green and sustainable
Protein aggregates
Purification

ABSTRACT

Systematic development of a temperature-controlled isocratic process for one-column low-salt hydrophobic interaction chromatography (HIC) of proteins employing a travelling cooling zone reactor (TCZR) system, is described. Batch binding and confocal scanning microscopy were employed to define process conditions for temperature-reversible binding of bovine serum albumin (BSA) which were validated in pulse-response temperature switching HIC experiments, before transferring to TCZR-HIC. A thin-walled stainless-steel column mounted with a movable assembly of copper blocks and Peltier elements (travelling cooling zone, TCZ) was used for TCZR-HIC. In pulse-response TCZR-HIC, 12 TCZ movements along the column desorbed 86.3% of the applied BSA monomers in 95.3% purity depleted >6-fold in 2–4 mers and nearly 260-fold in higher molecular weight (HMW) species. For continuous TCZR-HIC, the TCZ was moved 49–58 times during uninterrupted loading of BSA feeds at 0.25, 0.5 or 1 mg·mL^{-1}. Each TCZ movement generated a sharp symmetrical elution peak. In the best case, (condition 1: 0.25 mg·mL^{-1} BSA; >17 mg BSA applied per mL of bed) the height of TCZ elution peaks approached pseudo-steady midway through the loading phase with no rise in baseline UV280 signal between peaks. Peak composition remained constant averaging 94.4% monomer, 5.6% 2–4 mers and <0.05% HMW. Monomers were recovered in quantitative yield depleted >3.1 fold in 2–4 mers and 92-fold in HMW species cf. the feed (63.6% monomers, 21.8% 2–4 mers, 14.6% HMW). However, increasing the BSA concentration to 1 mg·mL^{-1} (condition 2) or employing a fouled HIC column with 0.5 mg·mL^{-1} BSA (condition 3) compromised monomer purification performance.

1. Introduction

Chromatographic operations are indispensable in the downstream processing of biotherapeutics, but their sustainability is coming under increasing scrutiny [1-3]. Adsorption chromatography can be hugely expensive. Traditionally employed approaches exacerbate these costs, and importantly exhibit poor green credentials. Batchwise single-column operation, for example, is characterised by low productivity, excessive buffer and water consumption and associated levels of waste for disposal post-manufacture [4-9]. Such concerns drive the bioprocess industry's growing interest in continuous manufacture [10]. Newer continuous chromatography formats promise significant and well-documented benefits cf. batch chromatography, namely increased capacity/resin productivity and process efficiency, lower operational costs, improved scalability, smaller physical footprints and reduced water consumption and environmental impact [3,4,6,7,10-18]. The transition from batch to continuous chromatography is currently hindered by the latter's greater complexity [13,16]. However, a rarely mentioned core problem is that large volumes of different buffers are employed during the sub-steps (equilibrating, washing, eluting,

* Corresponding author.
E-mail address: o.r.t.thomas@bham.ac.uk (O.R.T. Thomas).
[1] Present address: Technical Operations, Thermo Fisher Scientific, 8 Calthorpe Road, Birmingham, B15 1QT, UK.

https://doi.org/10.1016/j.chroma.2024.465212
Received 10 June 2024; Received in revised form 23 July 2024; Accepted 24 July 2024
Available online 25 July 2024

Table 1
Langmuir parameters for experiments shown in Fig. 1.

Batch	Lot number (ligand density)	Φ (°C)	q_{max} (mg·mL^{-1})	K_d (mg·mL^{-1})	R^2	q_{max}/K_d (-)	k'_Φ (-)	Δq_Φ (mg·mL^{-1})
A	10,281,131 (44 μmol·mL^{-1})	10	4.84 ± 0.65	5.88 ± 1.53	0.97	0.82	8.67	2.2
		21	4.95 ± 0.46	2.70 ± 0.58	0.96	1.83		
		40	7.04 ± 0.47	0.99 ± 0.25	0.94	7.11		
B	10,309,247 (47 μmol·mL^{-1})	10	4.40 ± 0.60	5.03 ± 1.22	0.98	0.87	10.16	2.7
		21	6.35 ± 0.77	3.30 ± 0.70	0.99	1.92		
		40	6.72 ± 0.44	0.76 ± 0.20	0.93	8.84		
C	10,317,570 (50 μmol·mL^{-1})	10	5.67 ± 1.20	4.35 ± 1.51	0.98	1.30	6.97	1.1
		21	5.06 ± 0.50	2.65 ± 0.61	0.98	1.91		
		40	6.52 ± 0.40	0.72 ± 0.19	0.93	9.06		
Müller & Franzreb (2012)	Unspecified	10	4.1	5.0	–	0.82	10.78	2.7
		25	4.7	1.67	–	2.82		
		40	6.8	0.77	–	8.84		

cleaning) with each generating waste. Solutions to this issue should improve the greenness and sustainability of chromatographic operations employed for biotherapeutics manufacture [5,19].

Hydrophobic interaction chromatography (HIC) is powerful and gentle technique for intermediate purification and polishing chromatography of proteins, [20-28] nucleic acids [21,29,30] and viruses [21, 31-33]. However, its reliance on very high concentrations of kosmotropic salts (e.g., ammonium sulphate) typically employed to promote binding [20,34-37] creates problems that escalate at manufacturing scales. These include: (i) the costs associated with intermediate sample preparation steps that may be required to reduce the salt concentration before the next process step; [38] (ii) ammonium sulphate is highly corrosive to stainless steel equipment; [39,40] and that (iii) large amounts of salts, especially ammonium sulphate and potassium phosphate, pose serious environmental concerns that render their disposal in municipal waste water very expensive [41].

An obvious solution to the above is to employ suitable replacements for kosmotropic salts. Gagnon [38] proposed glycine, but other additives [42] also invite attention. Further options are to eradicate [40,43] or minimize [44,45] the reliance of HIC on high concentrations of kosmotropic salts. In the specific case of monoclonal antibodies (mAbs) the triad combination of 'no-salt HIC, very hydrophobic stationary phases and flow through operation' represents an attractive option for selective removal of more hydrophobic aggregates from less hydrophobic mAbs; prior optimisation of mobile phase pH is required in each case [40,43]. Müller and Franzreb [45] described a novel and potentially generic solution for intermediate purification by low-salt HIC which involved using temperature to control adsorption-desorption equilibria.

The general effects of temperature on HIC are well known, i.e., high temperatures enhance binding and lower temperatures undermine it, promoting desorption [46-49]. It is somewhat surprising therefore that there are very few reports on the practical use of temperature modulation in HIC to switch between binding and elution states [50-52]. For example, Muca and coworkers [51] employed step changes in temperature and salt concentration to fractionate a multicomponent protein mix of bovine serum albumin (BSA), α-chymotrypsinogen, lysozyme and myoglobin, while Müller and Franzreb's [45] study aimed to use temperature in combination with low salt concentrations to reduce process costs and address the sustainability and green failings of HIC as it is currently practiced. Their approach involved: (i) screening the effect of temperature (10–40 °C) in low ammonium sulphate concentrations (0.1–0.5 M) on protein adsorption of BSA to HIC media; (ii) deriving Langmuir and thermodynamic parameters to identify the HIC matrix and ammonium sulphate concentration showing the strongest temperature influence; (iii) performing back-to-back multicycle temperature-driven adsorption-desorption runs in a column under isocratic conditions; and (iv) demonstrating that 'temperature only' mediated fractionation of protein mixtures at low salt concentration is possible.

Looking to the long-term future of bioprocess scale adsorption chromatography we introduced single-column continuous chromatography formats operated under isocratic conditions [5,19,53]. In these systems stainless-steel columns are mounted with travelling Peltier devices which transiently cool [5,53] or heat [19] defined regions or zones of the contained adsorbent bed as they migrate along the length of the column (note, no change in buffer composition is required). In this way discrete 'local' changes in bed temperature are used to control adsorption–desorption equilibria; in the standard case, driving elution of bound species from the support into the mobile phase, and exiting the column once the Peltier device passes the column exit [5,19,53]. This allows for uninterrupted loading of feedstock protein to the column, whilst simultaneously moving the cooling/heating zone along it in repeated fashion. In past demonstrations we employed: (i) thermoresponsive cation exchange media in a travelling cooling zone reactor (TCZR) system for continuous fractionation of a binary mixture of the proteins bovine serum albumin (BSA) and bovine lactoferrin; [53] and (ii) a commercially available thermoresponsive rProtein A matrix in a travelling heating zone reactor (THZR) system for three different monoclonal antibody (mAb) downstream processing applications, i.e., continuous mAb concentration, quasi-continuous mAb purification and quasi-continuous buffer exchange [19].

In this work we extend the repertoire of travelling cooling systems to HIC of proteins in low-salt buffers building on previous work by Müller and Franzreb [45] employing BSA and Butyl Sepharose 4 Fast Flow. Specifically, we describe batch binding experiments allied with confocal laser scanning microscopy (CLSM) to confirm optimal conditions for trialling low-salt HIC processes that employ 'cooling only' to effect elution, test the separation concept in pulse-response HIC experiments before transferring to batch and continuous TCZR-HIC to purify BSA monomers from larger and more hydrophobic forms.

2. Materials and methods

2.1. Materials

Butyl Sepharose™ 4 Fast Flow media (Table 1), Superdex 200 Increase, 300/10 GL size exclusion column, Gel Filtration Cal Kit High Molecular Weight, Blue Dextran 2000, and single-use PD-10 desalting columns packed with Sephadex G-25 were obtained from Cytiva UK Ltd (Little Chalfont, Bucks, UK). Bovine serum albumin (BSA, Cat. no. A7906, lyophilized powder, ≥98% by agarose gel electrophoresis) was acquired from Merck KGaA (Darmstadt, Germany) and used without further purification. Other chemicals supplied by Merck included the following: ammonium sulphate (Cat. No. A4418, ≥99% purity), disodium hydrogen phosphate (Cat No. S0876, ≥99%), sodium bicarbonate (Cat. No. S8875, ≥99.5%), sodium chloride (Cat. No. S/3120/63, >99.5%), Oxoid™ Phosphate Buffered Saline (PBS) tablets (Cat. No. BR0014G, >99%), sodium hydroxide (Cat. No. S0845, anhydrous ≥98%), hydrochloric acid (Cat. No 320,331, ACS reagent, 37%), absolute ethanol (Cat. No. E/0650DF/17, >99.8%), and acetone (Cat. No.

270,725, HPLC grade, ≥99.9%). Invitrogen™ Alexa Fluor™ 647 NHS Ester (Succinimidyl Ester) (Cat. No. A20006) and Invitrogen™ anhydrous DMSO (Cat. No D12345) for fluorophore tagging of BSA were purchased from Thermo Fisher Scientific (Waltham, MA, USA). All buffers and solutions were freshly made with purified water from a Sartorius arium® advance EDI Pure Water System (Sartorius AG, Göttingen, Germany), adjusted to the desired pH using 1 M NaOH or 1 M HCl and Fisherbrand accumet XL200 pH and conductivity metre (Fischer Scientific UK, Loughborough, Leics, UK), filtered through 0.22-μm pore MF-Millipore™ membrane filters (Fischer Scientific), and degassed for chromatography experiments.

2.2. Batch adsorption experiments

In batch binding tests, 125 μL portions of 40% (*v/v*) slurries Butyl 4 Sepharose Fast Flow matrices, previously equilibrated with 50 mM sodium phosphate buffer, pH 7.5 variously supplemented with ammonium sulphate (hereafter abbreviated to AS), were mixed with 125 μL aliquots of varying initial BSA concentration made up in the same buffer) and incubated at 10, 21, or 40 °C with shaking at 1100 rpm in an Eppendorf Thermomixer comfort shaker (Eppendorf SE, Hamburg, Germany) for 1 h. After an additional 0.5 h at the selected temperature without shaking, adsorbent particles were sedimented by pulse centrifugation (2000 g, 30 s) in a VWR ministar centrifuge (Radnor, PA, USA), and the supernatants were carefully removed and analysed for residual protein content (Section 2.7). The equilibrium BSA loadings on supports (q^*) were computed from the differences in initial (c_0) and equilibrium (c^*) bulk phase protein concentrations, and where appropriate the resulting q^* vs. c^* data were fitted to the simple Langmuir model (Eq. (1)):

$$q^* = \frac{q_{\max} c^*}{K_D + c^*} \tag{1}$$

where q^* and c^* represent the equilibrium concentrations of adsorbed and liquid-phase protein respectively; $q_{\max}$ is the maximum protein binding capacity of the support; and K_D is the dissociation constant. Data were fitted to the model using the χ^2 minimization procedure of OriginPro® 2022 software (OriginLab Corporation, Northampton, MA, USA).

2.3. Preparation of dye conjugated BSA

BSA was fluorescently labelled with Alexa Fluor 647, an amine-reactive dye selected for its resistance to quenching at high degrees of labelling and to photobleaching, [54] using the manufacturers' recommended protocol. Dye-labelled BSA conjugates were separated from unreacted dye by SEC using PD-10 columns. Fractions containing both dye and protein were pooled, analysed (Section 2.7) and employed in CLSM studies (Section 2.4).

2.4. Confocal laser scanning microscopy (CSLM)

CSLM was used to observe combined influences of AS concentration and temperature on distribution of BSA in Butyl Sepharose 4 Fast Flow beads. Portions (125 μL) of a 40% (*v/v* slurry) of Butyl Sepharose™ 4 Fast Flow (Batch B) pre-equilibrated for 1 h in 50 mM sodium phosphate buffer pH 7.5 supplemented with 0.3 – 1.5 M AS were incubated with a 125 μL aliquots of 8 mg·mL^{-1} protein solutions (comprising a 1:100 mix of dye-conjugated BSA to native unlabelled BSA) in the same buffers in screw-capped vials protected from light at Φ = 10, 21 and 40 °C. After 1.5 h of mixing at 1100 rpm in a Thermomixer (Eppendorf SE, Hamburg, Germany), the supports were recovered from solution by low-speed pulse centrifugation (2000 *g*, 10 s) in a Mini Star Silverline microfuge (VWR International, Lutterworth, Leics, UK), washed (3 × 200 μL) and re-suspended in 0.5 mL of the same binding buffer at the binding temperature. Aliquots (20 μL) of the support slurries were pipetted onto microscope slides, covered with a coverslip, and analysed with a Zeiss LSM 780 microscope using an LD LCI Plan-NEOFLUAR 25 × /0.8 oil-immersion objective (Carl-Zeiss Microscopy GmbH, Jena, Germany). The samples were excited with the system's helium/neon 633 nm laser line (gain = 500, 2% laser power) and images were captured with ZEN 2.1 software (Carl-Zeiss Microscopy GmbH, Jena, Germany), and then processed (Section 2.7).

2.5. Pulse-response HIC experiments

The effect of temperature on elution under binding conditions (50 mM sodium phosphate pH 7.5 supplemented with 0.5 M AS) was evaluated by a pulse-response chromatography using Tricorn™ 5/50 columns (Cytiva, Marlborough, MA, USA) containing 1 mL beds of Butyl Sepharose 4 Fast Flow 'Batch B' connected to an ÄKTAprime plus system (GE Healthcare, Uppsala, Sweden). BSA pulses (2 mg in 0.50 mL) were applied to equilibrated columns submerged in a Techne TE-10A circulating water bath (Thermo Fisher Scientific, Waltham, MA, USA) held at Φ = 40 °C. After washing with at ~4 CV of binding buffer at the same temperature, columns were either stripped with 20% (*v/v*) ethanol at Φ = 40 °C or transferred to an iced-water cooling bath (maintained at Φ = 10 °C) to trigger elution before stripping with 20% (*v/v*) ethanol at Φ = 10 °C. Flow leaving the columns was continuously conductivity and UV absorbance at 280 nm. The temperatures of the water and iced-water baths were continuously logged (Elitech RC-5+, Elitech Technology Inc., San Jose, CA, USA) during experiments and remained constant.

2.6. TCZR chromatography experiments

2.6.1. Basic set-up

A brief description of the TCZR set-up is given below. For more detail the reader is referred to our previous studies [5,53]. The TCZR system comprises: (i) an insulated temperature-controlled cabinet; (ii) a vertically aligned stainless steel column (internal diameter = 6 mm, length = 360 mm); and (iii) the column mounted travelling cooling zone (TCZ) arrangement, which surrounds a discrete zone of the column. The walls of the column are only 1 mm thick to ensure rapid and homogenous radial heat transfer. With PTFE capped stainless steel adaptors inserted into both ends of the column the internal volume for accommodating the stationary phase can be reduced to 2.83 mL (length = 100 mm). The TCZ is a 'Club sandwich-like' arrangement of three copper blocks and two Peltier elements (Type TB-109-1,4-1,5CH, Kryotherm, St, Petersburg, Russia), flanked top and bottom by aluminium heatsink blocks. By attaching the TCZ to a linear motorized axis (Festo AG, Munich, Germany) controlled by dedicated PC based software (Festo Configuration Tool, FCT) it can be moved along the column in either direction at a velocity of 0.1 to 40 mm·s^{-1}. The Peltier elements of the TCZ are connected to a MTTC-1410 thermoelectric temperature controller (Laird Thermal Systems, Morrisville, NC). The temperatures of the cabinet/column and TCZ are monitored in real-time using Pt100 resistance thermometers linked to LabView™ Software (National Instruments, Austin, TX, USA). The TCZR apparatus is controlled by an external computer running LabView software, and Festo control panel, where the TCZ velocity (v_c), linear motor position, and temperature (Φ) of the cabinet or cooling zone can be measured and modified.

2.6.2. General description and procedures

All TCZR-HIC experiments were conducted using an ÄKTA Explorer 100 Air chromatography workstation operated using Unicorn 5.1.1 software (GE Healthcare, Uppsala, Sweden). The separation column was packed with Butyl Sepharose™ 4 Fast Flow (Batch B) at 0.5 mL·min^{-1} (volume = 3.11 mL; length = 110 mm; compression factor = 1.09). In all experiments: (i) 50 mM sodium phosphate buffer pH 7.5 supplemented with 0.5 M AS was used for equilibration, binding, washing and TCZ elution steps; (ii) cabinet and TCZ temperatures were fixed at Φ = 40 ± 1 °C and 10 ± 1 °C respectively; (iii) v_c was 0.1 mm·s^{-1}; and (iv) a

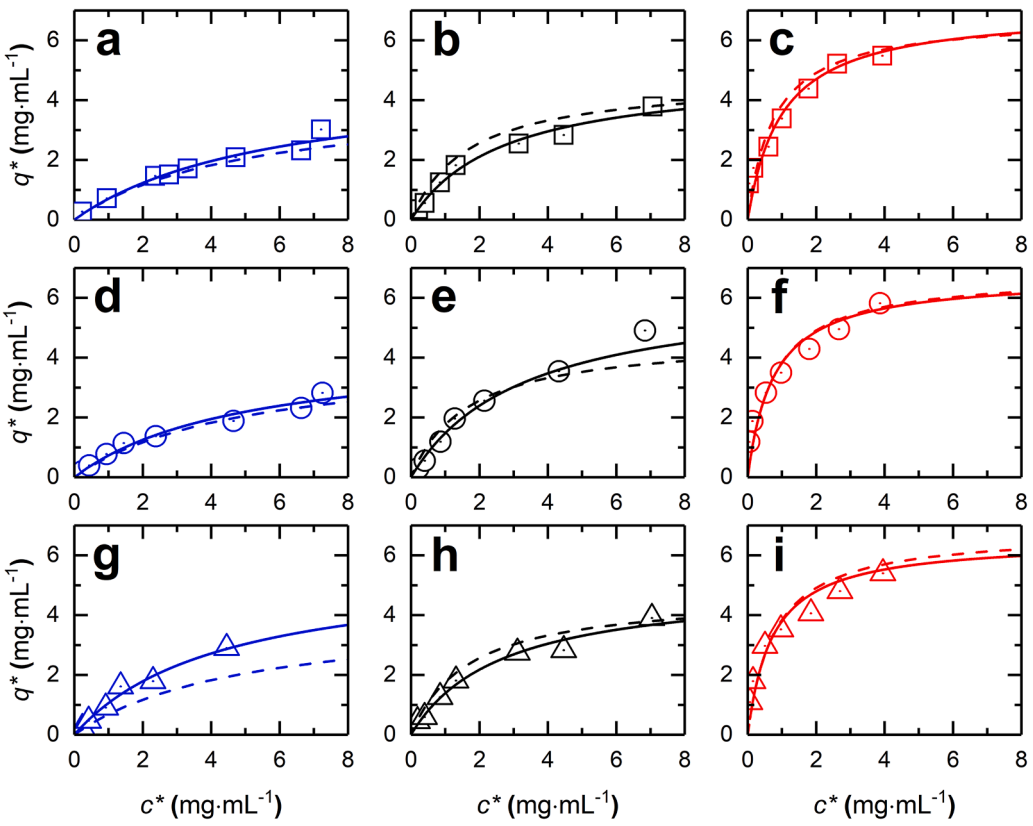

Fig. 1. Equilibrium isotherms for the adsorption of BSA to batches A (a – c; open squares), B (d – f; open circles) and C (g – i; open down-triangles) of Butyl Sepharose 4 Fast Flow tested in this study. The solid lines (blue = 10 °C; black = 21 °C; red = 40 °C) through the data points represent fitted Langmuir curves with parameter values presented in Table 1 and the dashed lines (blue = 10 °C; black = 25 °C; red = 40 °C) are simulated Langmuir curves for BSA adsorption to the batch of Butyl Sepharose 4 Fast Flow employed by Müller and Franzreb (2012).

constant volumetric flow rate of 0.18 mL·min^{-1} was used equating to a superficial mobile phase velocity, u, of 38.2 cm·h^{-1}. Assuming a settled bed voidage, ε_o, of 0.41 for 4% cross-linked Sepharose™ [55] the calculated bed voidage, ε, was ~0.36. Thus, the interstitial velocity, u_i (at $u = 38.2$ cm·h^{-1}) was 107.1 cm·h^{-1} or 0.30 mm·s^{-1}, i.e., 3 × faster than v_c (0.1 mm·s^{-1}). The interval between successive TCZ movements was varied by adjusting the start and end positions. For example, at $v_c = 0.1$ mm·s^{-1}, start and end positions 40 mm either side of the 110 mm high chromatographic bed correspond to a 31.67 min cycle time (190 mm of travel), whereas 5 mm displaced start and end points reduce the cycle time to 20 min (120 mm travel). Immediately on reaching the end position, the TCZ is rapidly returned to its starting position above the bed in immediate readiness for the next downward pass. The return velocity used in this work of 20 mm·s^{-1} adds an extra 6 s to a 20 min cycle time and 9.5 s to a 31.67 min cycle, giving peak-to-peak separation times of 20.1 min and 31.83 min.

In batch mode TCZR experiments, BSA (0.5 mL of 4 mg·mL^{-1}) was applied to pre-equilibrated beds of Butyl Sepharose 4 Fast Flow at Φ = 40 °C. The columns were then washed (3 CV) before initiating the first of 7 – 12 sequential movements of the TCZ along the column's full separation length. On completion of the TCZ's last movement columns were stripped using 20% (*v*/*v*) ethanol at Φ = 40 °C.

For continuous TCZR-HIC BSA loading and TCZ movements were performed concurrently. BSA was applied at Φ = 40 °C to fresh, regenerated or fouled (inadequately cleaned) Butyl Sepharose 4 Fast Flow columns at concentrations of 0.25, 1 and 0.5 mg·mL^{-1} respectively. A minimum of 58 TCZ cycles was conducted at regular intervals (20 or 21.8 min). Loading of BSA was maintained for 190 – 210 mL at which point the flow to columns was switched from BSA in buffer to buffer only whilst continuing TCZ operation for another 6 – 8 cycles, before administering 20% (*v*/*v*) ethanol to the columns at Φ = 40 °C. Between runs columns were cleaned with 1 M NaOH, washed with purified water and stored in 20% (*v*/*v*) ethanol.

Flow exiting all columns was continuously monitored for conductivity and UV absorbance at 280 nm, and all fractions generated during experiments were retained for SEC analysis (Section 2.7).

2.7. Analysis

Alex Fluor 647 dye and BSA concentrations in samples were determined in a DeNovix DS-11+ UV spectrophotometer (Wilmington, DE, USA) at wavelengths of 650 nm and 280 nm respectively.

CLSM data was analysed using ImageJ2 (Fiji) software [56]. Intensity vs. radial position profiles were extracted and plotted in OriginPro. For ease of visualisation [57] images of individual chromatography beads are shown in the "Hot Cyan" colour scale available in ImageJ Fiji.

After packing and prior to each new TCZR-HIC run bed quality was assessed by comparing peak asymmetry factors (A_s). For this, tracer pulses (50 µL of 0.8 M NaCl) were injected onto Butyl Sepharose 4 Fast Flow columns operated at 0.18 mL·min^{-1} and employing 0.4 M NaCl as the mobile phase. A minimum of three measurements were performed and A_s was calculated using the ÄKTA Explorer's Unicorn software version 5.1. In all TCZR experiments, regardless of bed history, A_s values were close to 1. Areas under peaks in chromatograms were calculated using OriginPro's Peak Analyser (OriginLab Corporation, Northampton, MA, USA) tool and were subsequently converted to mass (1 mg·mL^{-1} BSA gives a UV 280 signal of 115 mAU).

The compositions of feed solutions and peak fractions collected during TCZR-HIC chromatography were analysed by SEC analysis using a Superdex 200 increase, 300/10 GL column (Cytiva, Marlborough, MA, USA) previously calibrated with Ovalbumin (44 kDa), Conalbumin (75

kDa), Aldolase (158 kDa), Ferritin (440 kDa), Thyroglobulin (669 kDa) and Blue Dextran 2000 (2000 kDa). Syringe filtered samples were injected onto the column via a 500 μL sample loop. Chromatography was performed at 0.5 mL·min^{-1} using PBS (10 mM phosphate, 137 mM NaCl, 2.7 mM KCl, pH 7.4) as the mobile phase and the UV absorbance of the exiting flow was monitored at 215 and 280 nm. Three elution peaks were observed in BSA feed samples with apparent molecular weights corresponding to monomers, small oligomers (dimers, trimers, and tetramers), and higher molecular weight (HMW) species (larger oligomers and soluble aggregates).

3. Results and discussion

In their study Müller and Franzreb [45] screened four differently functionalised HIC media for the binding of BSA at temperatures, Φ, between 10 and 40 °C in a 50 mM sodium phosphate pH 7 buffer variously supplemented with low concentrations (0.1 – 0.5 M) of AS. The authors: (i) noted that temperature dependency is inversely correlated with hydrophobicity of the matrix; (ii) singled out Butyl Sepharose 4 Fast Flow as most promising for further investigation of temperature dependency in HIC; (iii) employed van't Hoff analysis, applied to collected isotherm data, to calculate thermodynamic contributions to BSA binding, highlighting the key import of ΔS cf. ΔG and q_{max}; and (iv) recommended binding (high) and desorption (low) temperatures are ideally selected so that ΔG flips its sign from strongly negative at the higher temperature to positive at the lower temperature.

3.1. BSA adsorption on Butyl Sepharose 4 Fast Flow

Protein binding in HIC is well known to correlate with alkyl chain length and ligand density [25,58-60]. Müller and Franzreb [45] did not specify the ligand density (or lot number from which this could be identified) of the Butyl Sepharose 4 Fast Flow used in their work. In this study, three different lots (designated A – C) with ligand densities ranging from 44 – 50 μmol·mL^{-1} were screened in batch adsorption isotherms conducted with BSA in phosphate buffer containing 0.5 M AS (Fig. 1, Table 1) with two objectives in mind, i.e., identify: (i) the adsorbent best matching the matrix used by Müller and Franzreb [45] for ease of comparison; and more importantly (ii) the matrix displaying the strongest temperature dependency. Here, temperature dependency is described by two parameters, i.e., Δq_Φ, the difference in binding capacity at 40 °C and 10 °C [45] and k'_Φ, the ratio of the initial slopes q_{max}/K_d at 40 °C and 10 °C. At 40 °C BSA binding to all batches of Butyl Sepharose 4 FF (Figs. 1c, 1f and 1i, Table 1) is very similar (q_{max} = 6.5 – 7 mg·mL^{-1}, K_d = 0.7 – 1.0 mg·mL^{-1}, q_{max}/K_d = 7.1 – 9.1). A reduction in temperature to 21 °C substantially weakens binding (Figs. 1b, 1e and 1h), but the same commonality is retained for batches A–C (q_{max} = 5.0 – 6.35 mg·mL^{-1}, K_d = 2.7 – 3.3 mg·mL^{-1}, q_{max}/K_d = 1.8 – 1.9). Reducing the temperature yet further to 10 °C exposes differences in BSA binding characteristics between the batches (Fig. 1a, d and g). Batch C (50 μmol·mL^{-1}), likely the most densely derivatised of the four batches, exhibits stronger binding character (e.g., q_{max}/K_d = 1.30 cf. 0.8–0.9; Table 1), which compromises its temperature dependency (Δq_Φ = 1.1 mg·mL^{-1}, k'_Φ = 7) cf. the rest (Δq_Φ = 2.2 – 2.7 mg·mL^{-1}, k'_Φ = 8.7 – 10.8). Batch B was selected for use in all subsequent studies as it displayed the strongest temperature dependent BSA binding of the three batches of Butyl Sepharose 4 Fast Flow batch, closely matching the behaviour previously reported by Müller and Franzreb [45] for a different batch of the same matrix.

3.2. Temperature dependency window for BSA on Butyl Sepharose 4 Fast Flow

To identify operating windows/limits of temperature dependency of BSA binding to Butyl Sepharose 4 Fast Flow the combined influence of AS concentration and temperature was explored in batch binding and

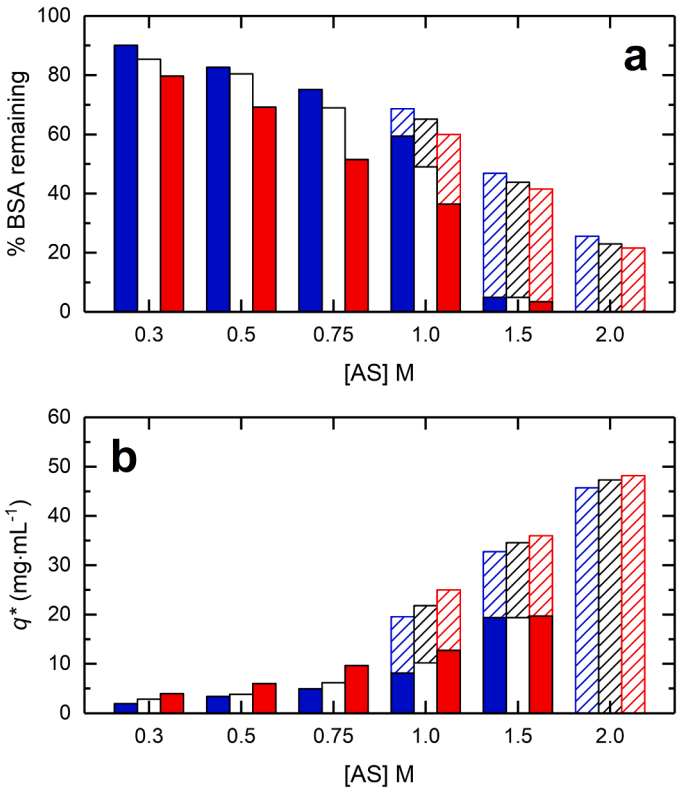

Fig. 2. Combined influence of temperature and AS concentration on BSA binding to Butyl Sepharose 4 Fast Flow at challenges of 20 (filled bars; 0.3 – 1.5 M AS) and 62 (hatched bars; 1–2 M AS) mg BSA per mL of support. Binding temperatures of 40, 21 and 10 °C are indicated by red, black, and blue respectively. Panels a and b respectively show the% of BSA remaining in solution and binding capacity plotted against AS concentration.

CLSM studies. At a challenge of 20 mg BSA per mL adsorbent in the presence of 0.3 M AS only 9.9 – 20.3% of the protein was adsorbed (Fig. 2a). BSA binding capacities were low (1.92, 2.84 and 3.94 mg·mL^{-1} at 10, 21 and 40 °C respectively), but a clear advantage of higher temperature was observed, i.e., the binding capacity at 40 °C was 2.05-fold higher than at 10 °C (Fig. 2b; Δq_Φ = 2.02 mg·mL^{-1}). With increasing AS concentration capacities rose steeply in roughly linear fashion (Fig. 2b). The advantage of high temperature on binding persisted at 0.5 M (6.0 mg·mL^{-1} at 40 °C cf. 3.38 mg·mL^{-1} at 10 °C, i.e., 1.78-fold; Δq_Φ = mg·mL^{-1}), 0.75 M (9.64 mg·mL^{-1} at 40 °C cf. 4.94 mg·mL^{-1} at 10 °C, i.e., 1.95-fold higher; Δq_Φ = 4.7 mg·mL^{-1}) and 1 M added salt concentrations (12.72 mg·mL^{-1} at 40 °C cf. 8.12 mg·mL^{-1} at 10 °C, i.e., 1.57-fold higher; Δq_Φ = 4.6 mg·mL^{-1}) but was lost almost completely at 1.5 M AS (19.68 mg·mL^{-1} at 40 °C cf. 19.38 mg·mL^{-1} at 10 °C; Δq_Φ = 0.3 mg·mL^{-1}). A similar trend was observed at the higher challenge of 62 mg BSA per mL adsorbent conducted at high added AS concentrations of 1 – 2 M, i.e., capacities increasing with increasing salt and accompanied by gradual loss of temperature dependency (Δq_Φ falling from 5.44 mg·mL^{-1}at 1 M added salt to 2.46 mg·mL^{-1} at 2 M AS). When expressed as percentages of capacities at 40 °C these values of Δq_Φ are small, i.e., reflecting binding capacity differences of 21.76% at 1 M AS dropping to 5.11% at 2 M added AS. Thus, for the present system (BSA, Butyl Sepharose 4 Fast Flow) a thermally driven process employing high temperature (40 °C) binding and low temperature (10 °C) for elution is only viable with low AS concentrations (0.3 – 0.75 M).

CLSM images arising from equilibrium binding (t = 1.5 h) of Alexa Fluor 647 conjugated BSA to Butyl Sepharose 4 Fast Flow as functions of temperature (10, 21 and 40 °C) and AS concentration (0.3 – 1.5 M) are shown in Fig. 3, and the corresponding fluorescence intensity scans are presented in Fig. 4. The general influence of temperature on

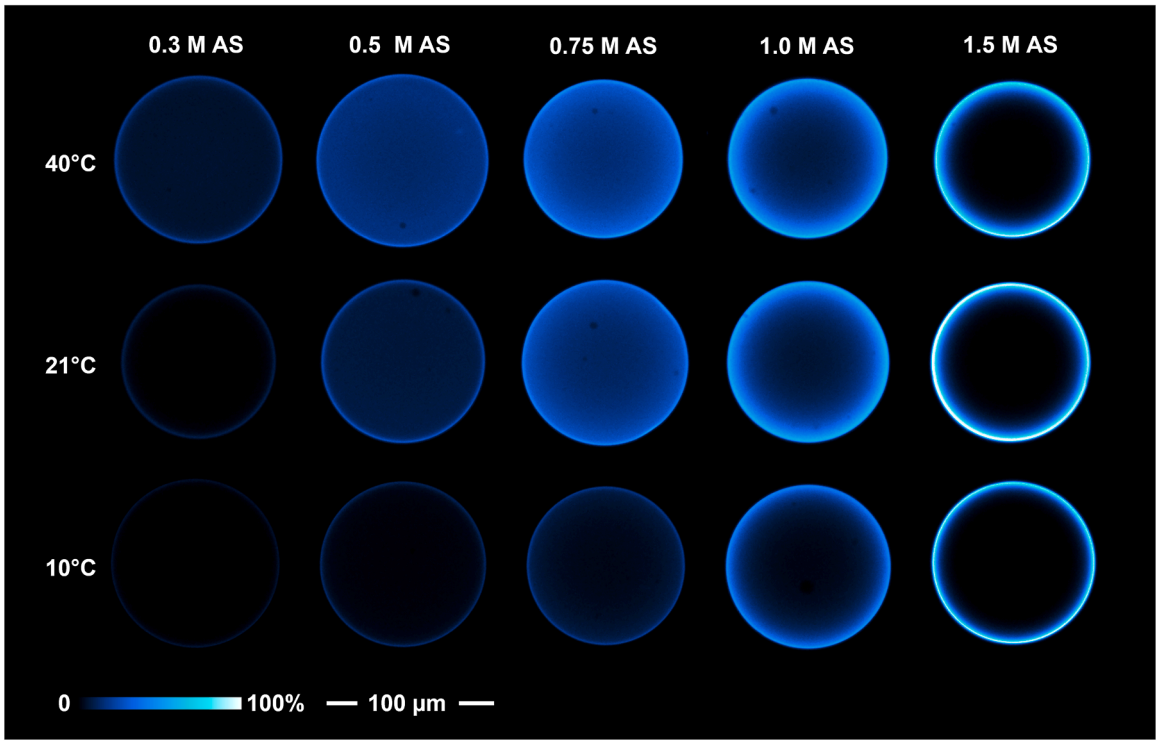

Fig. 3. CLSM images of temperature dependent binding of Alexa Fluor 647-tagged BSA to Butyl Sepharose 4FF beads at AS concentrations of 0.3 – 1.5 M and temperatures of 10, 21 and 40 °C. See text for details.

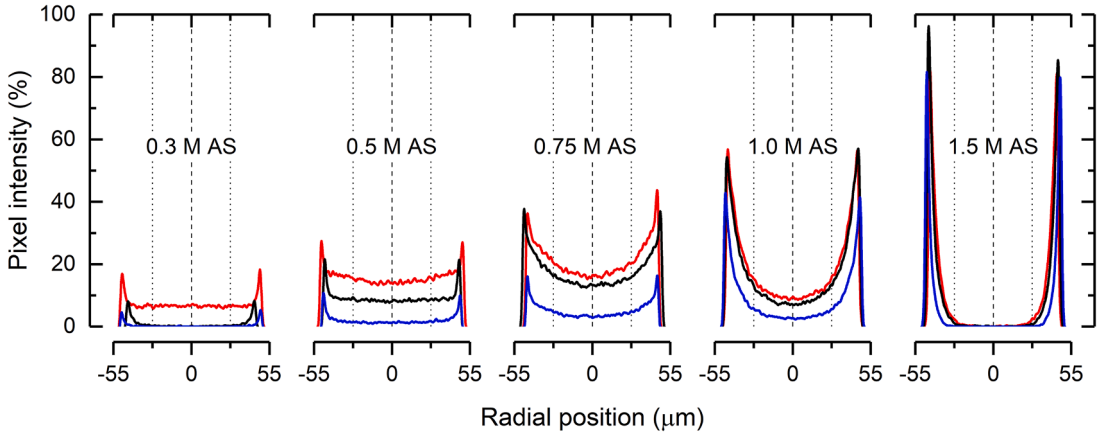

Fig. 4. Intensity profiles of beads taken from the left-to-right horizontal midpoint of each bead featured in Fig. 3. Pixel intensity represents image brightness, and is the raw output from the CLSM, reported as grey value. The red, black, and blue traces represent binding temperatures of 40, 21 and 10 °C respectively.

fluorescence intensity and intraparticle distribution of adsorbed BSA in Butyl Sepharose 4 Fast Flow beads can be appreciated at all AS concentrations but is most noticeable below 0.75 M added salt. Temperature plays a secondary role cf. salt when high concentrations of the latter (1 and 1.5 M) are employed. Post binding and prior to CLSM analysis samples were washed at the binding temperature. At 10 °C in the presence of 0.3 – 0.75 M AS concentrations and at 21 °C in 0.3 M AS, binding is weak; thus, much of the adsorbed BSA is lost during the wash step and fluorescence is fainter than expected based on scrutiny of Fig. 2b. At 40 °C in 0.3 M AS BSA is transported into the centre of the bead (Figs. 3 and 4) and raising the salt concentration to 0.5 M increases bead fluorescence uniformly across the bead diameter. At the lower temperatures (21 °C and especially 10 °C) BSA binding is very feeble in 0.3 and 0.5 M AS; the difference in fluorescence (Fig. 3) and pixel intensity (Fig. 4) at 40 and 10 °C in 0.5 M added salt is particularly striking and lends support to the selection of this AS concentration for all subsequent work (i.e., pulse-response HIC and TCZR-HIC experiments). Marked and progressive changes in fluorescence intensity and distribution occur as the salt concentration is raised beyond 0.75 M, regardless of temperature, i.e., sharp adsorption fronts develop, separating saturated shells from empty cores, indicating that intraparticle transport of BSA is dominated by hindered pore diffusion [61,62]. At these high AS concentrations (>1 M) extensive unfolding, strong binding, and aggregation of BSA in outer regions of the Butyl Sepharose 4 Fast Flow adsorbent particles [63] blocks the pores preventing further transport to the bead interiors.

3.3. *Pulse-response HIC*

Prior to trialling TCZR-HIC, pulse-response experiments (Fig. 5) were

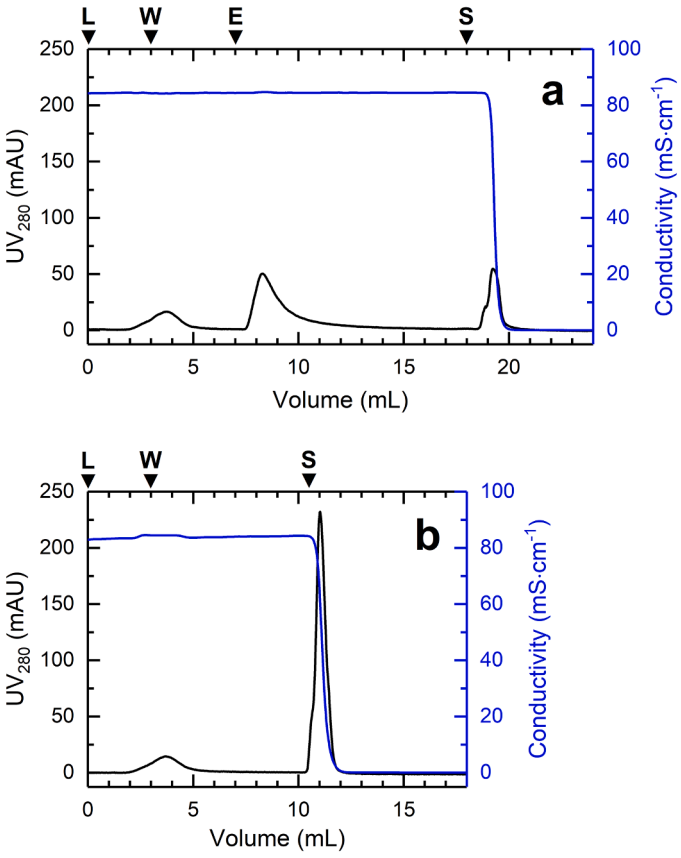

Fig. 5. Pulse-response chromatography of BSA on Butyl Sepharose 4FF columns. BSA (2 mg equiv. 33% EBC) was loaded to the columns in sodium phosphate buffer pH 7.5 supplemented with 0.5 M AS at Φ = 40 °C and washed at the same temperature. Columns were then: (a) eluted by being immersed in an ice bath (Φ = 10 °C) before stripping with 20% (*v*/*v*) ethanol (Φ = 10 °C); or (b) stripped with 20% (*v*/*v*) ethanol at Φ = 40 °C. Loading, wash, elution, and strip phases are indicated arrow heads and the letters L, W, E and S respectively UV absorbance and conductivity traces are respectively indicated by black and blue traces.

Table 2
Evaluation of process performance during pulse response HIC of BSA corresponding to Fig. 5.

Experiment	Φ = 40 °C		Φ = 10 °C		*% Mass balance*
	Eluted (%)	Firmly bound (%)	Eluted (%)	Stripped (%)	
Bath @ 40 °C (Fig. 5a)	16.9	83.1	–	87.1	*104.0*
Baths @ 40 & 10 °C (Fig. 5b)	17.7	82.3	56.0	23.3	*97.0*

conducted using a small glass column packed with Butyl Sepharose 4 Fast Flow submerged in a water bath held at 40 °C. BSA was supplied as 2 mg pulses (equivalent to 33% of the equilibrium binding capacity of 6 mg·mL^{-1}) to the equilibrated bed at 0.18 mL·min^{-1} in 50 mM sodium phosphate, pH 7.5 containing 0.5 M AS. The beds were then washed with the same buffer at the same temperature. Under these conditions <20% of the absorbed BSA (Fig. 5, Table 2), identified by Jungbauer et al. [64] as weakly bound native BSA, elutes isocratically as a small broad peak (<3 CV). By contrast retained BSA, elutable by lowering the salt concentration or stripping with 20% (*v*/*v*) ethanol, is predominantly unfolded [45,63,64]. Fig. 5b and Table 2 show that a substantial fraction (two-thirds) of this tightly bound BSA can be desorbed without change in mobile phase composition, simply by transferring the column to an ice

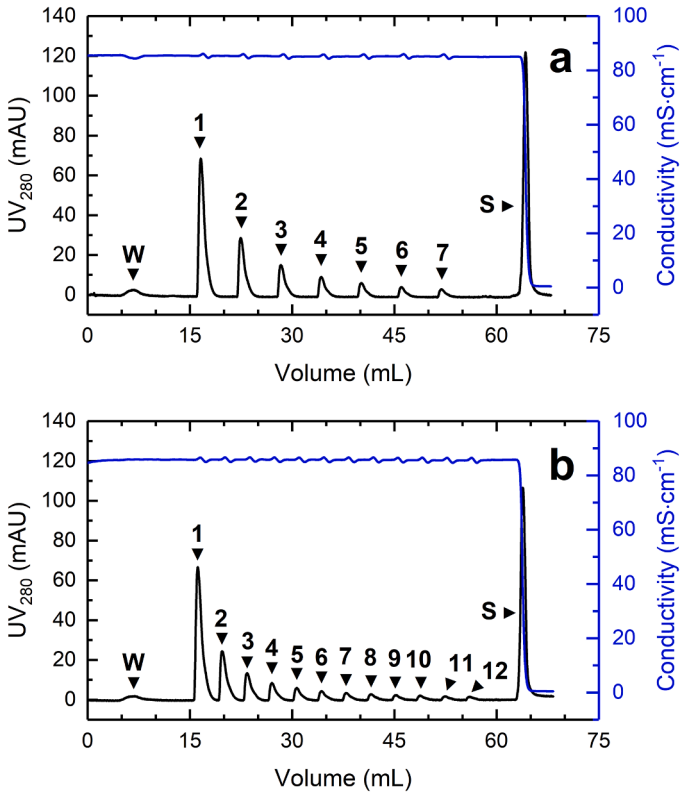

Fig. 6. Chromatograms arising from TCZR tests with Butyl Sepharose 4 Fast Flow in 0.5 M AS in 50 mM sodium phosphate buffer pH 7.5 employing multiple movements of the TCZ at a velocity v_c of 0.1 mm·s^{-1}. Columns were loaded with 2 mg of BSA (0.5 mL of 4 mg·mL^{-1}) and washed at the binding temperature (40 °C) prior to initiating the first of seven (a) or twelve (b) sequential movements of the TCZ. Arrow heads with letters or numbers indicate wash (W), TCZ elution (1 – 12) and strip (S) peaks. UV absorbance and conductivity signals are respectively indicated by black and blue traces.

water bath maintained at ~10 °C. Cooling the column in this manner generated a broad strongly tailing elution peak (extending over >6 CV) containing 56% of initially bound BSA. Firmly bound BSA, i.e., that not eluted by cooling, was desorbed from the column in a third sharp peak (23.2% recovered) by stripping with 20% (*v*/*v*) ethanol. Immediate stripping of the column with 20% (*v*/*v*) ethanol post isocratic elution (i.e., omitting the cooling step) resulted in a sharp strip peak (Fig. 5a) of greater magnitude (87.1% recovery). No further protein was recovered by cleaning the beds with 1 M NaOH.

3.4. Batch mode TCZR-HIC of BSA

With the benefits of cooling as a means of elution clearly established, temperatures for binding and elution were transferred to TCZR HIC

Table 3
Evaluation of process performance for batch TCZR-HIC of BSA corresponding to Fig. 6.

Experiment	% BSA recovered				*% Mass balance*
	Feed (Φ = 40 °C)	Wash (Φ = 40 °C)	TCZ elution cycles (Φ = 10 °C)	Strip (Φ = 10 °C)	
7 × 31.83 min cycles (Fig. 6a)	100	2.7	64.4	45.7	*112.8*
12 × 20.1 min cycles (Fig. 6b)	100	2.3	66.1	39.0	*107.3*

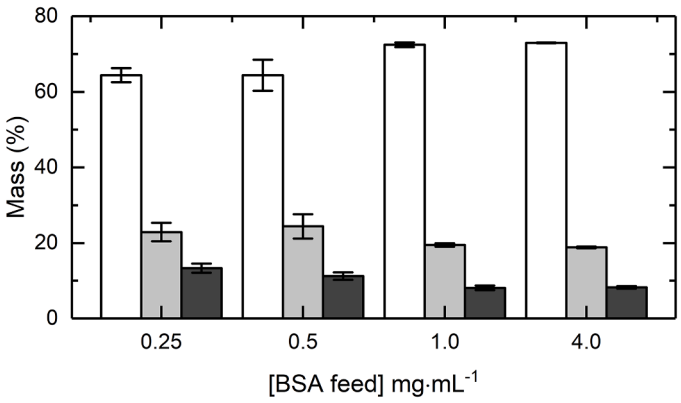

Fig. 7. Influence of BSA concentration in the feed on composition determined by SEC. BSA was prepared in 50 mM sodium phosphate supplemented with 0.5 M AS. Key: monomers (white bars); 2–4 mers (pale grey bars); HMW species (dark grey).

operation in batch and subsequently continuous modes using 3.4 mL beds of Butyl Sepharose 4 Fast Flow packed in a thin-walled stainless-steel column (ID = 6 mm), cabinet and TCZ temperature of 40 °C and 10 °C respectively and mobile phase of 0.3 mm·s^{-1} and TCZ velocity of 0.1 mm·s^{-1}. Analogous to pulse-response experiments (Fig. 5) in batch TCZR-HIC (Fig. 6), 2 mg BSA were applied to equilibrated beds at 40 °C in 50 mM sodium phosphate pH 7.5 containing 0.5 M AS and the columns were subsequently irrigated with the same buffer at the same flowrate.

The first peak in both chromatograms (Fig. 6a and b) is of weakly adsorbed native BSA and is much smaller (<3% of the load, Table 3) than those observed in the bath pulse-response experiments (<20%, Fig. 5, Table 2), and likely relates to the >3-fold lower BSA loading employed as a percentage of equilibrium binding capacity, i.e., 9.8% cf. 33%. Previously, Müller and Franzreb [45] observed that while the degree of BSA unfolding on Butyl Sepharose 4 Fast Flow columns is practically independent of the amount loaded at temperatures of 10 and 25 °C, at 40 °C the extent of unfolding increases markedly at low BSA loadings; supporting earlier findings from Muca et al. [52] that increasing temperature strongly enhances BSA unfolding and retention in HIC. TCZ migration along the column was initiated shortly after weakly bound BSA had eluted from the column, and the first thermally eluted peak was generated as the TCZ passed the column exit. At this point the TCZ reverses its direction of travel and is quickly returned (v_c = 20 mm·s^{-1}) to the top of the bed in readiness for its next descent. In the first experiment (Fig. 6a) a total of seven THZ movements or cooling cycles were performed. Each travel of the TCZ is accompanied by a sharp elution peak and small blip in the conductivity profile [19]. The size of thermal elution peaks drops with each successive cycles (Fig. 6, Table 3) as the portion of thermally elutable BSA bound to the bed is progressively reduced with each elution. TCZR mediated elution from Butyl Sepharose 4 Fast Flow in the stainless-steel column compared favourably with immersion of the whole bed (contained in a glass column) in the 10 °C ice bath. Combined TCZ cycles recovered >64% of the loaded BSA cf. 56% by cooling the entire bed. The first TCZ cycle accounted for 48% of the thermally eluted BSA, and each subsequent cycle desorbed diminishing amounts. In the second batch TCZR HIC experiment (Fig. 6b) the TCZ 'start' and 'end' positions were adjusted (while maintaining the same v_c of 0.1 mm·s^{-1}) to reduce the cycle time from 31.83 to 20.1 min. In this manner five more travels could be conducted

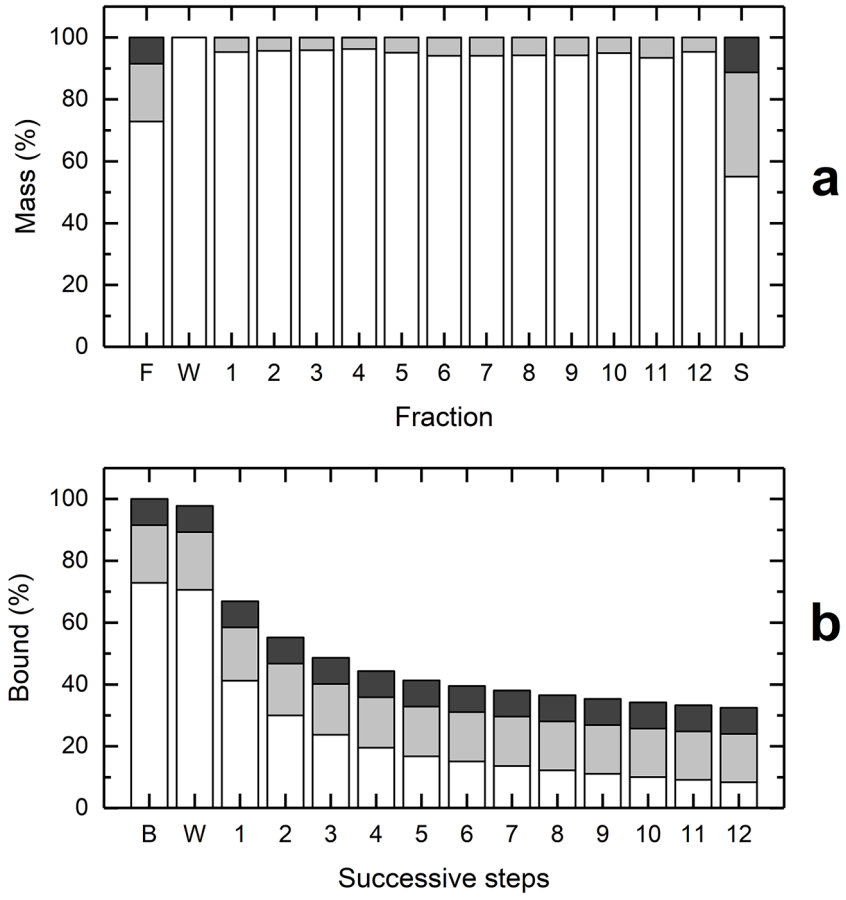

Fig. 8. (a) SEC analysis of fractions and (b) calculated changes in mass of adsorbed BSA species during TCZR-HIC (Fig. 6b). Key: feed (F); wash (W); TCZ elution peaks (1 – 12); strip (S); monomers (white bars); 2–4 mers (pale grey bars); HMW species (dark grey).

Table 4
Tracking of BSA monomer, dimer and HMW species during TCZR-HIC on Butyl Sepharose 4 Fast Flow (Fig. 6b).

Fraction	BSA (mg)	BSA composition (%)			BSA composition (mg)			Monomer		DF (-)	
		Monomers	2–4 mers	HMW	Monomers	2–4 mers	HMW	Recovery (%)	PF (-)	2–4mer	HMW
Feed (F)	2.0	72.9	18.7	8.5	1.46	0.37	0.17	100	1.0	1.0	1.0
Wash (W)	0.05	100	0	0	0.05	0	0	3.2	1.37	–	–
Elution pool (1–12 incl.)	1.32	95.3	4.6	0.05	1.26	0.06	<0.001	86.3	1.31	6.12	257
Strip (S)	0.78	55.1	33.6	11.3	0.43	0.26	0.09	29.5	0.76	1.42	1.92
Sum of all fractions	2.15				1.73	0.32	0.09				
% Mass balance	*107.3*				*119.0*	*86.60*	*52.4*				

Compositions were determined by SEC analysis (Fig. 8a). Key: PF = purification factor; DF = depletion factor.

within approximately the same period (i.e., 12 cf. 7) reducing the peak-to-peak distance from ~5.8 mL (Fig. 6a) to ~3.6 mL (Fig. 6b). A small improvement in thermal elution yield of BSA was observed, i.e., twelve combined cooling cycles recovered 66.1% cf. 64.4% (Table 3). In both runs the first TCZ cycles accounted for nearly 50% of the thermally eluted BSA (48%, Fig. 6a, cf. 46%, Fig. 6b), and each subsequent cycle desorbed decreasing quantities of BSA. Taken collectively it appears that: (i) more than 60% of the BSA retained on Butyl Sepharose 4 Fast Flow at 40 °C in 0.5 M AS can be recovered by a 30 °C thermal shift to 10 °C; (ii) the TCZR system is able to match/surpass the elution performance achieved by cooling the entire bed; (iii) a significant portion of BSA (ca. 40%) remains bound after cooling, but is easily recovered by stripping with 20% (*v/v*) ethanol.

3.5. SEC analysis of feedstocks and fractions from batch TCZR-HIC of BSA

BSA solutions contain a dynamic mix of interconverting monomeric and multimeric structures of closely related but non-identical molecules; [65,66] the amounts of each depend on solvent properties (e.g., buffer pH, salt concentration and type of salt), temperature and protein concentration. To gain a deeper understanding of TCZR-HIC performance, feedstocks and peak fractions were analysed by SEC. The BSA concentration of feedstocks used in chromatographic studies varied between 0.25 to 4 mg·mL^{-1}.

Fig. 7 shows that the composition remained essentially the same at 1 and 4 mg·mL^{-1} BSA (i.e., 72.4 cf. 72.9% monomers; 19.5 cf. 18.8% 2–4 mers; 8.1 cf. 8.2% HMW), but at lower BSA concentrations (0.25 and 0.5 mg·mL^{-1}) the monomer content dropped to 63.4% at the expense of increased presence of small oligomers (22.9 – 24.4%) and HMW (11.2 –

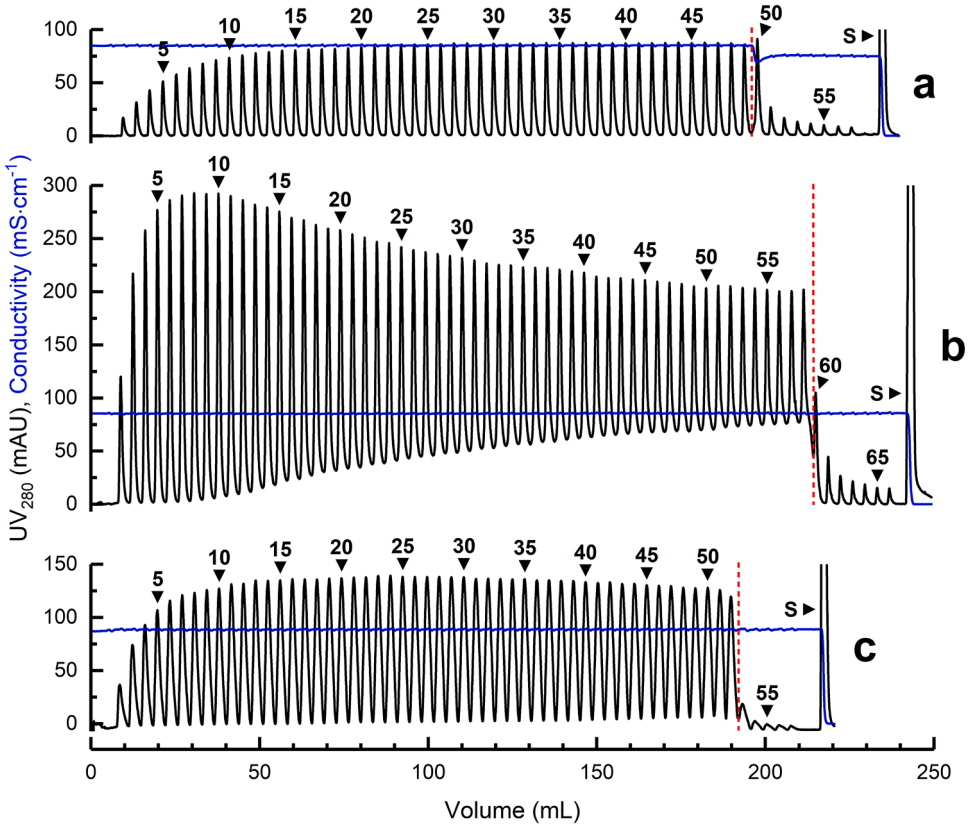

Fig. 9. Chromatograms arising from continuous TCZR-HIC tests with Butyl Sepharose 4FF in 0.5 M AS in 50 mM sodium phosphate buffer pH 7.5 employing 58+ movements of the TCZ at a velocity v_c of 0.1 mm·s^{-1}. BSA was continuously supplied at: (a) 0.25 mg·mL^{-1} to a fresh column (condition 1); (b) 1 mg·mL^{-1} to a regenerated column (condition 2); and (c) 0.5 mg·mL^{-1} to a fouled column (condition 3). Labelled arrow heads indicate sequential TCZ elution and the ethanol strip (S) peak, and the dashed red lines indicate termination of BSA supply marking the transition from continuous to batchwise operation. The distance travelled by the TCZ was 130 mm (a) or 120 mm (b, c) resulting in a peak-peak cycle times of 21.78 min or 20.1 min respectively. UV absorbance and conductivity signals are respectively indicated by black and blue traces.

13.3%). These findings, though initially counterintuitive, accord with observations that aggregation of BSA is more prevalent in dilute solutions, indicating no inherent tendency of the molecule to aggregate [65, 67,68]. Madeira and coworkers [65] hypothesized there were two distinct monomeric forms in solution, one with no tendency to aggregate the other exhibiting increasing aggregation tendency on dilution, and that dilution increases the relative proportion of the latter which in turn drives increased aggregation. Fig. 8a and Table 4 respectively show SEC composition analysis of the feed (4 mg·mL^{-1}) and pooled peak fractions from the TCZR-HIC run in Fig. 6b, and key mass balance and purity data for the same experiment. The feed composed <73% monomers, <19% small oligomers and >8% HMW, and the wash peak contained only monomer (Fig. 8a). All twelve TCZ eluted peaks were essentially composed of 95% monomers and 5% small oligomers. No significant differences in composition were noted from one TCZ cycle to the next other than trace levels of HMW (0.06 ± 0.01%) detected in the first few TCZ elution cycles, but not in the last seven elution peaks. In stark contrast, 2–4 mer and HMW combined accounted for nearly 45% of the BSA in ethanol strip peak.

The mass balance for overall BSA recovery in the experiment closed to >107% (Table 4). Monomers in TCZ pool of elution peaks were >95% pure and, based on the improbable assumption of 'no changes in composition' during chromatography, were recovered in 119% yield. The mass balances for recovered small oligomers (86.6%) and HMW (52.4%) did not close. From this it follows that some portion of oligomeric and higher order BSA desorbed from the column during regeneration with 20% (*v/v*) ethanol is converted back to monomeric form (see 3.6).

3.6. Continuous TCZR-HIC

Having established the effectiveness of the TCZ in selectively eluting essentially only monomeric forms whilst accumulating more hydrophobic multimers/HMW aggregates during batch mode HIC, we next employed TCZR-HIC in continuous mode at three different BSA feed concentrations (Fig. 9) to explore its potential/define its limits as a protein aggregate removal step. In previous work using TCZR and THZR systems respectively configured with smart thermoresponsive cation exchange adsorbents [53] and a thermoresponsive rProtein A matrix [19] we were able to match the rates of the protein loading/ binding with those of thermal elution. This resulted in elution peaks reaching a steady maximum height returning to the baseline between peaks. In both studies the travelling devices were operated over 6 – 9 cycles and steady state was typically observed after the 2 – 4 cycles depending on the target protein concentration in the feed. Given the findings from batch experiments, best illustrated by Fig. 8b, that tightly binding higher order species accumulate on the column and their binding status is not affected by cooling, at some point during continuous supply of BSA to the bed the column's capacity for 2–4 mer and HMW will be reached, and these species will begin to appear in the exiting flow along with monomer. At this point feeding should stop, so that the column can be regenerated (by stripping with 20% *v/v* ethanol followed by NaOH) in readiness for the next round of processing (continuous feeding of BSA and TCZ elution of monomer). It also follows that the working capacity for monomer elution by TCZ cooling must decline at some point during extended operation, meaning that true quasi-steady state operation is not possible. To test the above reasoning in this work feed was continuously administered at different BSA concentrations (0.25, 1 and 0.5 mg·mL^{-1}) to freshly packed (Fig. 9a), regenerated (Fig. 9b) or fouled (Fig. 9c) beds of Butyl Sepharose 4 Fast Flow and operation was extended to 58+ travels. Feeding of BSA in buffer (phosphate containing 0.5 M AS) to the beds was maintained for 190 – 210 mL during which the TCZ had moved 49 – 58 times before switching to buffer only. TCZ movements were continued at the same frequency another 5 – 9 times mimicking batch mode operation. Bound BSA not eluted by the TCZ was desorbed after the last movement by stripping with 20% (*v/v*) ethanol.

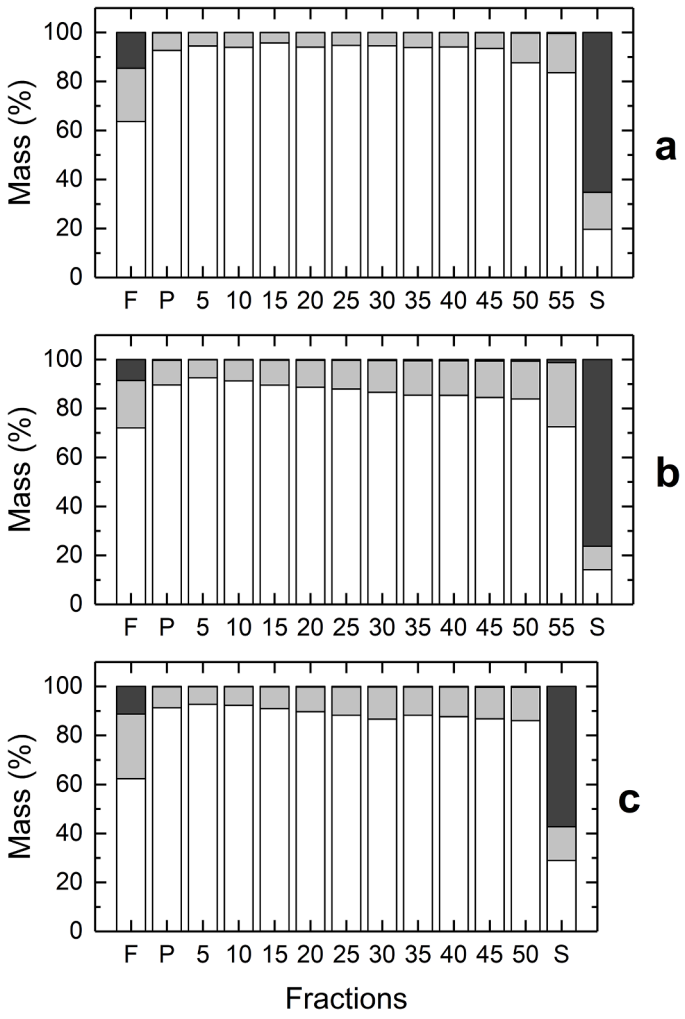

Fig. 10. SEC analysis on selected fractions taken during continuous TCZR-HIC of BSA (Fig. 9) on (a) fresh (condition 1), (b) regenerated (condition 2) and (c) fouled (condition 3) Butyl Sepharose 4 Fast Flow columns. Key: feed (F); elution pool (P); selected elution peaks (5 – 55); strip (S); monomers (white bars); 2–4 mers (pale grey bars); HMW species (dark grey bars).

Comparison of individual eluted peaks within the chromatograms (Fig. 9) indicates a certain time is required before maximum peak height/area is reached and that raising the BSA feed concentration speeds its acquisition. For example, at 0.25, 0.5 and 1 mg·mL^{-1} BSA in the feed maximum peak size were reached at peaks 27 (Fig. 9a), 23 (Fig. 9c) and 8 (Fig. 9b) respectively. Other notable aspects discussed below are the UV_{280} baseline signal, eluate composition during the continuous loading-unloading phase, purification performance and mass balance closures, and the width and shape of TCZ elution peaks.

3.6.1. Continuous TCZR-HIC on 'clean' HIC columns (Conditions 1 & 2)

The baseline signal remained flat for the 'fresh bed + 0.25 mg·mL^{-1} BSA' experiment (condition 1; Fig. 9a), during which 49 movements of the TCZ had been completed during the continuous loading-unloading phase followed by a further 8 without feeding (simulating batchwise operation; Section 3.4). SEC analysis of every 5th peak (5, 10, 15, 20, 25, 30, 35, 40 and 45) during the continuous loading-unloading part of the run (until and including peak 49) confirmed high monomer purity (av. 94.4 ± 0.6%) across all TCZ elution peaks; 2–4 mer and HMW respectively accounted for 5.6 ± 0.6% and <0.05 ± 0.025% of the BSA population (Fig. 10a). On terminating the supply of BSA increased levels of 2–4 mer and HMW were detected in peaks 50 (12.1% 2–4 mer, 0.21% HMW) and 55 (16.0% 2–4 mer, 0.38% HMW); thus, monomer purity

Table 5
Tracking of BSA monomers, 2–4 mers and HMW species during continuous TCZR-HIC on Butyl Sepharose 4FF (Fig. 9). Compositions were determined by SEC analysis (Fig. 10). Key: PF = purification factor; DF = depletion factor.

Condition 1: Fresh bed supplied with 0.25 mg·mL^{-1} BSA (Figs. 9a and 10a).

Fraction	BSA (mg)	BSA composition (%)			BSA composition (mg)			Monomer		DF (-)	
		Monomer	2–4 mer	HMW	Monomer	2–4 mer	HMW	Recovery (%)	PF (-)	2–4 mer	HMW
Feed (F)	48.9	63.6	21.8	14.6	31.1	10.7	7.1	100	1.0	1.0	1.0
Elution pool (P)	34.1	92.7	7.1	<0.2	31.6	2.4	0.05	101.6	1.46	3.07	92.1
Strip (S)	11.5	19.7	15.0	65.3	2.3	1.7	7.5	7.3	0.31	1.45	0.22
Sum of all fractions	45.6				33.9	4.1	7.5				
% Mass balance	*93.1*				*108.9*	*38.8*	*105.6*				

Condition 2: Regenerated bed supplied with 1.0 mg·mL^{-1} BSA (Figs. 9b and 10b).

Fraction	BSA (mg)	BSA composition (%)			BSA composition (mg)			Monomer		DF (-)	
		Monomer	2–4 mer	HMW	Monomer	2–4 mer	HMW	Recovery (%)	PF (-)	2–4 mer	HMW
Feed (F)	213.7	72.1	19.4	8.5	154.0	41.4	18.3	100	1.0	1.0	1.0
Elution pool (P)	188.2	89.6	10.1	<0.3	168.7	19.0	0.5	109.5	1.24	1.92	30.5
Strip (S)	23.4	14.2	9.6	76.2	3.3	2.2	17.8	2.2	0.20	2.02	0.11
Sum of all fractions	211.6				172.0	21.2	18.4				
% Mass balance	*99.00*				*111.7*	*51.2*	*100.6*				

Condition 3: Fouled bed supplied with 0.5 mg·mL^{-1} BSA (Figs. 9c and 10c).

Fraction	BSA (mg)	BSA composition (%)			BSA composition (mg)			Monomer		DF (-)	
		Monomer	2–4 mer	HMW	Monomer	2–4 mer	HMW	Recovery (%)	PF (-)	2–4 mer	HMW
Feed (F)	96.1	62.4	26.3	11.3	60.0	25.3	10.9	100	1.0	1.0	1.0
Elution pool (P)	112.4	91.3	8.5	<0.2	102.7	9.6	0.2	171.2	1.46	3.09	59.5
Strip (S)	10.2	29.0	13.7	57.3	3.0	1.40	5.8	4.9	0.46	1.92	0.20
Sum of all fractions	122.6	62.4			105.6	11.0	6.0				
% Mass balance	*127.6*	*91.3*			*176.1*	*43.4*	*55.6*				

was noticeably reduced in these fractions (Fig. 10a). These reductions can be explained at least in part by a pump valve error which led to dilution of the mobile phase, lowering the conductivity from 85 mS·cm^{-1} to 70 – 76 mS·cm^{-1} (Fig. 9a) thereby weakening adsorption of bound 2–4 mer and HMW BSA. As the mass contributions of peaks 50 – 58 were small (1.89 mg) cf. all preceding peaks (32.21 mg) monomer purity of the pool dropped only slightly to 92.7% (Table 5, condition 1). Of the 48.9 mg BSA applied (31.1 mg monomer, 10.7 mg 2–4 mers, 7.1 mg HMW), 34.1 mg was recovered by the TCZ cooling cycles (31.6 mg of which was monomer), and stripping post TCZ with 20% (*v/v*) ethanol closed the mass balance to >93% (Table 5, condition 1). Monomers were recovered in high yield and purity, depleted 3.1-fold with respect to 2–4 mers and 92-fold in HMW species.

Increasing the BSA concentration continuously applied to same column to 1 mg·mL^{-1}, after cleaning and re-equilibration (condition 2), compromised TCZ elution performance. Approximately 30 mL (30 mg) into loading, roughly coincident with the 8th travel of the TCZ (which issued the tallest peak in the run at 2.6 mg BSA), the baseline UV signal started drifting upwards, while the peak height diminished, creating a striking chromatographic profile (reminiscent of the dorsal fin of a Sailfish or Marlin). The mass passing in the 'bleed' (area between the original baseline line and the TCZ eluted peaks) grew throughout the loading phase to represent 45% of the total BSA eluted on completion (TCZ elution peaks accounted for 55% of the total). Note, the rising baseline/increasing bleed does not reflect increasing passive passage of BSA through the bed. Rather it implies bound monomers are displaced back into the mobile phase by more hydrophobic and avidly binding 2–4 mer and HMW BSA species. With gradually increasing supply to the bed available capacity for adsorbing BSA is consumed by tighter binding species, thus levels of more readily desorbed monomers drop, which accounts for diminishing height of TCZ elution peaks observed through the loading-unloading phase of Fig. 9b. SEC analysis of fractions generated after the 5th travel of the TCZ confirmed gradual reduction in monomer purity primarily at the expense of 2–4 mer, though increasing HMW contamination of the eluate is discernible from peak 20 onwards (Fig. 10b). Approximately 214 mg of BSA (72.1% monomers, 19.4% 2–4 mers, 8.5% HMW) was applied in this experiment (Figure 9b; Table 5, condition 2) of which >188 mg was eluted (184 mg during feeding, 4.2 mg once feeding had stopped) and a further 23.4 mg was recovered in the 20% (*v/v*) ethanol strip. BSA monomers were recovered in the eluate in high yield but at lower purity (89.6%) cf. that observed with the 0.25 mg·mL^{-1} feed (92.7%; Table 5, condition 1). For 'clean' beds continuously challenged with BSA at 0.25 and 1 mg·mL^{-1} (Fig. 9a and b) mass balances for monomer exceeded 100% (Table 5, conditions 1 and 2) while those for 2–4 mers fell far short, i.e., 38.8% (Table 5, condition 1) and 51.2% (Table 5, condition 2). As noted earlier (Section 3.5) the process of stripping with ethanol likely dissociates some higher order BSA structures, 2–4 mers in particular, to monomeric forms.

Plots of BSA composition vs accumulated mass of BSA supplied to the HIC columns (Fig. 11) provide a clearer picture of how eluate composition changes during continuous TCZR HIC of BSA on Butyl Sepharose 4 Fast Flow as a function of feed concentration.

At 0.25 mg BSA per mL the composition of the elute remained relatively stable throughout the loading-unloading phase (averaging 94.4% monomer, 5.6% 2–4 mer, <0.05% HMW). For the 1 mg·mL^{-1} condition, monomer accounted for 92.5% of the BSA present in peak 5 (Fig. 11, first data point) and was generated before the baseline began to rise (peak 8; Fig. 9b). Thereafter the contribution of monomers in elution fractions fell steadily to reach <84% at peak 50 (Fig. 11, last data point), paralleling the increasing appearance of 2–4 mer and HMW species (Figure 11; >15% and >0.6% respectively) and rising baseline 'bleed' and shrinking 'monomer-rich' peaks observed in Fig. 9b.

Realistically, at any given BSA feed concentration continuous operation of TCZR-HIC should continue to the point where the baseline starts to rise, as this point should coincide with deterioration of performance, e.g., marked by a drop in monomer purity (Figs. 10 and 11), whereupon the bed should be regenerated before initiating the next round of continuous TCZR HIC. That point was after only ~30 mg had been applied (~10 mg BSA per mL of bed) at 1 mg·mL^{-1} (Fig. 9b) but was not reached at 0.25 mg·mL^{-1} (Fig. 9a), signifying in this case, a safe/

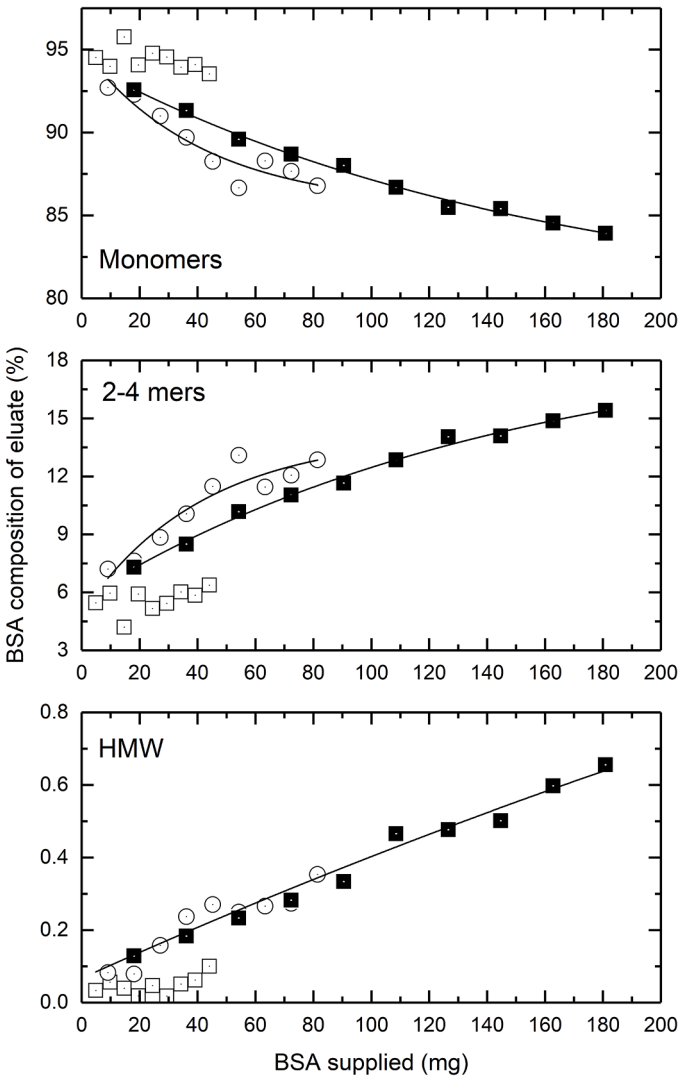

Fig. 11. BSA eluate composition vs. BSA supplied during continuous TCZR-HIC of BSA (Fig. 9, loading phase only). Key: fresh column fed with 0.25 mg·mL^{-1} BSA (open squares); regenerated column fed with 1 mg·mL^{-1} BSA (filled squares); fouled column fed with 0.5 mg·mL^{-1} BSA (open circles).

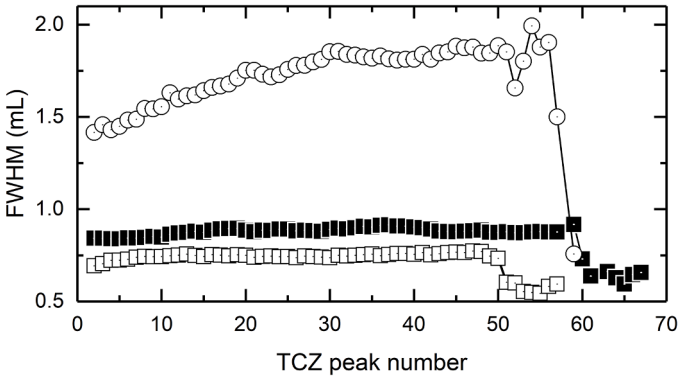

Fig. 12. Peak width vs. TCZ peak number during continuous TCZR-HIC of BSA (Fig. 9). Key: fresh column fed with 0.25 mg·mL^{-1} (open squares); regenerated column fed with 1 mg·mL^{-1} BSA (filled squares); fouled column fed with 0.5 mg·mL^{-1} (open circles).

conservative loading capacity of >50 mg or 17 mg of BSA per mL of matrix, per operating cycle, featuring >50 movements of the TCZ with each unloading 0.7 – 0.8 mg of >94% pure monomer .

3.6.2. *Continuous TCZR-HIC on a fouled HIC column*

The chromatogram for continuous TCZR-HIC of BSA at 0.5 mg·mL^{-1} on a fouled bed of Butyl Sepharose 4 Fast Flow (i.e., one previously exposed to 100 mg of BSA, cleaned and stored in 20% (*v/v*) ethanol, but not subjected to 1 NaOH) appears superficially similar to those conducted with freshly cleaned beds of the same matrix, with maximum peak heights roughly correlating with BSA feed concentration and gradually decreasing peak magnitude after the 23rd pass of the TCZ (Fig. 9c). However, there are salient differences, i.e., the UV_{280} baseline rises continuously from the outset (reaching 8 mAU at ~190 mL accounting for 11.5 mg or 10.2% of the BSA eluted), and the TCZ elution peaks are much wider/less sharp, and their width gradually increases as more BSA is supplied to the bed (Fig. 12). For example, for the clean columns full-width-at-half-maximum (FWHM) values during loading remain relatively constant at 0.76 ± 0.01 mL and 0.84 ± 0.02 mL at 0.25 mg·mL^{-1} and 1 mg·mL^{-1} respectively. For the fouled column FWHM starts at 1.42 mL for the first elution peak and climbs to a maximum of 1.99 mL for the 53rd. On switching to batch operation FWHM drops steeply in all cases consistent with reduced mass in the elution peaks. In total, 96.1 mg of BSA was supplied to the fouled column (Table 5, condition 3), 112.4 mg was collected in the elution pool (of which 102.7 mg was monomer representing $a > 1.7$ increase cf. the feed) and 10.2 mg in the strip fraction, i.e., considerably more came off the column than was applied (mass balance = 127.6%) reflecting that BSA accumulated on the column in previous trial runs (not shown) appeared in the exiting flow of the run in Fig. 9c. The impact of this 'extra source' of BSA on eluate composition can be seen in Figs. 10c and 11. Monomer purity in the eluate from the fouled column fed with 0.5 mg·mL^{-1} deteriorated more readily than for the clean column fed with twice the BSA concentration in plots of composition vs. BSA supplied (Fig. 11), largely due to enhanced levels of 2–4 mers. For example, monomer purities dropped below 90% after supply of just 25 mg BSA to the fouled column (condition 3) cf. >50 mg to the clean column (condition 2), but the gap between the two conditions appears to close at higher BSA supply, i.e., beyond ~70 mg. Hence, the fouled column fed with 0.5 mg·mL^{-1} BSA delivered comparable purification performance (Table 5, condition 3) to that of the freshly regenerated bed of identical matrix operated with twice the BSA concentration (Table 5, condition 3).

4. Conclusions

In earlier work, Müller and Franzreb [45] showed how temperature alone could be used to control the sorption behaviour of BSA in HIC. Novel TCZR/THZR systems capable of performing continuous temperature-controlled adsorption chromatography in a single column were subsequently developed and trialled for protein fractionation by ion exchange [5,53] and affinity separation [19].

In this study the systematic advance of continuous low-salt TCZR-HIC for the separation of protein monomers from higher order species is demonstrated. Suitable conditions for temperature reversible binding of BSA to Butyl Sepharose 4 Fast Flow without any modulation of buffer composition were identified, from batch binding and CLSM studies mapping AS concentration and temperature combined, and confirmed in pulse-response temperature switching experiments, before successfully transferring to TCZR-HIC, first in batch and subsequently in continuous operating modes.

SEC analysis of BSA in TCZ eluted peaks generated during continuous TCZR-HIC revealed they were substantially purified with respect to monomer. In the best case (condition 1 employing the lowest BSA feed concentration of 0.25 mg·mL^{-1}) continuous TCZR-HIC operated at >17 mg BSA applied per mL of bed delivered monomeric BSA of >94% purity substantially depleted in higher order structures (5.6% 2–4 mer,

<0.05% HMW) cf. the initial feed (63.6% monomer, 21.8% 2–4 mer, 14.6% HMW), but raising the BSA feed concentration applied impaired both operational capacity and purity profile.

Ultimately, two factors compromise the effective use of continuous TCZR-HIC in this work, namely: (i) the low protein binding capacity of Butyl Sepharose 4 Fast Flow and other traditional HIC media, especially at low ionic strengths; [45,61] and (ii) the high content of strongly binding higher order species in BSA feeds, which accounted for 23 – 36.4% of the mass depending on the concentration employed. The low binding capacity issue calls for the development of new high-capacity media with heightened sensitivity to temperature [53,69-71]. Aggregate levels in mAbs post-capture are typically an order of magnitude lower than for BSA [72,73] and must be reduced to <1% in final mAb formulations [74]. It follows that TCZR-HIC might be attractive for removal of trace level soluble aggregates from monoclonal antibodies. Monoclonal antibodies are significantly more thermostable than BSA [75-80] meaning that higher temperatures could be used to enhance binding at low salt concentrations.

CRediT authorship contribution statement

Alexander Brean: Data curation, Investigation, Writing – original draft. **Tim W. Overton:** Supervision, Writing – review & editing. **Daniel G. Bracewell:** Funding acquisition, Supervision, Writing – review & editing, Methodology. **Matthias Franzreb:** Conceptualization, Methodology, Supervision, Writing – review & editing. **Owen R.T. Thomas:** Conceptualization, Formal analysis, Funding acquisition, Investigation, Methodology, Project administration, Resources, Supervision, Writing – original draft, Writing – review & editing.

Declaration of competing interest

The authors declare the following financial interests/personal relationships which may be considered as potential competing interests: Professor Owen R.T. Thomas reports financial support was provided by UK Engineering and Physical Sciences Research Council. If there are other authors, they declare that they have no known competing financial interests or personal relationships that could have appeared to influence the work reported in this paper.

Data availability

Data will be made available on request.

Acknowledgements

This work was supported by the UK Engineering and Physical Sciences Research Council (EPSRC) Centre for Doctoral Training in Emergent Macromolecular Therapies (EP/L015218/1). The authors acknowledge the expert technical assistance of Dr Alessandro Di Maio of the University of Birmingham's Advanced Light Microscopy Facility (BALM).

References

[1] T.N. Warner, T.N.S. Nochumson, Rethinking the economics of chromatography, BioPharm Int. 16 (2003) 58–60.
[2] M.C. Nweke, A.S. Rathore, D.G. Bracewell, Lifetime and aging of chromatography resins during biopharmaceutical manufacture, Trends Biotechnol. 36 (2018) 992–995.
[3] O. Khanal, A.M. Lenhoff, Developments and opportunities in continuous biopharmaceutical manufacturing, MAbs 13 (2021) e1903664.
[4] B. Linke, Y.C. Huang, D. Dornfeld, Establishing greener products and manufacturing processes, Int. J. Precis. Eng. Manuf. 13 (2012) 1029–1036.
[5] T.K.H. Müller, P. Cao, S. Ewert, J. Wohlgemuth, H. Liu, T.C. Willett, E. Theodosiou, O.R.T. Thomas, M. Franzreb, Integrated system for temperature-controlled fast protein liquid chromatography comprising improved copolymer modified beaded agarose adsorbents and a travelling cooling zone reactor arrangement, J. Chromatogr. A 1285 (2013) 97–109.
[6] P. Bunnak, R. Allmendinger, S.V. Ramasamy, P. Lettieri, N.J. Titchener-Hooker, Life-cycle and cost of goods assessment of fed-batch and perfusion-based manufacturing processes for mAbs, Biotechnol Prog. 32 (2016) 1324–1335.
[7] S.R. Madabhushi, J. Gavin, S. Xu, C. Cutler, R. Chmielowski, W. Rayfield, N. Tugcu, H. Chen, Quantitative assessment of environmental impact of biologics manufacturing using process mass intensity analysis, Biotechnol. Prog. 34 (2018) 1566–1573.
[8] K. Budzinski, M. Blewis, P. Dahlin, D. D'Aquila, J. Esparza, J. Gavin, S.V. Ho, C. Hutchens, D. Kahn, S.G. Koenig, R. Kottmeier, J. Millard, M. Snyder, B. Stanard, L. Sun, Introduction of a process mass intensity metric for biologics, N. Biotechnol. 49 (2019) 37–42.
[9] K. Budzinski, D. Constable, D. D'Aquila, P. Smith, S.R. Madabhushi, A. Whiting, T. Costelloe, M. Collins, Streamlined life cycle assessment of single use technologies in biopharmaceutical manufacture, N. Biotechnol. 68 (2022) 28–36.
[10] A. Jungbauer, P. Satzer, A. Duerauer, A. Azevedo, R. Aires-Barros, B. Nilsson, S. Farid, S. Goldrick, M. Ottens, M. Sponchioni, H.M.F. Lahore, Continuous downstream processing, Sep. Purif. Technol. 338 (2024) 126439.
[11] M. Pietrzykowski, W. Flanagan, V. Pizzi, A. Brown, A. Sinclair, M. Monge, An environmental life cycle assessment comparison of single-use and conventional process technology for the production of monoclonal antibodies, J. Clean. Prod. 41 (2013) 150–162.
[12] A.S. Rathore, H. Agarwal, A.K. Sharma, M. Pathak, S.J.P.B Muthukumar, Continuous processing for production of biopharmaceuticals, Prep. Biochem. Biotechnol. 45 (2015) 836–849.
[13] A.L. Zydney, Continuous downstream processing for high value biological products: a review, Biotechnol. Bioeng. 113 (2006) 465–475.
[14] X. Gjoka, R. Gantier, M. Schofield, Transfer of a three step mAb chromatography process from batch to continuous: optimizing productivity to minimize consumable requirements, J. Biotechnol. 242 (2017) 11–18.
[15] A.A. Shukla, L.S. Wolfe, S.S. Mostafa, C. Norman, Evolving trends in mAb production processes, Bioeng. Transl. Med. 2 (2017) 58–69.
[16] B. Somasundaram, K. Pleitt, E. Shave, K. Baker, L.H. Lua, Progression of continuous downstream processing of monoclonal antibodies: current trends and challenges, Biotechnol. Bioeng. 115 (2018) 2893–2907.
[17] H. Balfour, Continuous biomanufacturing – where are we now? Eur. Pharm. Rev. 26 (2021) 12–15.
[18] L. Gerstweiler, J. Bi, A.P.J. Middelberg, Continuous downstream bioprocessing for intensified manufacture of biopharmaceuticals and antibodies, Chem. Eng. Sci. 231 (2021) 116272.
[19] B. Ketterer, C. Moore-Kelly, O.R.T. Thomas, M. Franzreb, Integrated system for temperature-controlled fast protein liquid chromatography. III. Continuous downstream processing of monoclonal antibodies, J. Chromatogr. A 1609 (2020) 460429.
[20] S. Hjertén, Some general aspects of hydrophobic interaction chromatography, J. Chromatogr. A 87 (1973) 325–331.
[21] S. Hjertén, Hydrophobic interaction chromatography of proteins, nucleic acids, viruses, and cells on noncharged amphiphilic gels, Methods Biochem. Anal. 27 (1981) 89–108.
[22] T.W. Perkins, D.S. Mak, T.W. Root, E.N. Lightfoot, Protein retention in hydrophobic interaction chromatography: modeling variation with buffer ionic strength and column hydrophobicity, J. Chromatogr. A 766 (1997) 1–14.
[23] J.A. Queiroz, C.T. Tomaz, J.M.S. Cabral, Hydrophobic interaction chromatography of proteins, J. Biotechnol. 87 (2001) 143–159.
[24] M.E. Lienqueo, A. Mahn, J.C. Salgado, J.A. Asenjo, Current insights on protein behaviour in hydrophobic interaction chromatography, J. Chromatogr. B. 849 (2007) 53–68.
[25] B.C. To, A.M. Lenhoff, Hydrophobic interaction chromatography of proteins. I. The effects of protein and adsorbent properties on retention and recovery, J Chromatogr A (2007) 191–205.
[26] A.A. Shukla, B. Hubbard, T. Tressel, S. Guhan, D. Low, Downstream processing of monoclonal antibodies – application of platform approaches, J. Chromatogr. B 848 (2007) 28–39.
[27] S.M. Cramer, M.A. Holstein, Downstream bioprocessing: recent advances and future promise, Curr. Opin. Chem. Eng. 1 (2011) 27–37.
[28] S. Fekete, J.L. Veuthey, A. Beck, D. Guillarme, Hydrophobic interaction chromatography for the characterization of monoclonal antibodies and related products, J. Pharm. Biomed. Anal. 130 (2016) 3–18.
[29] M.M. Diogo, S. Ribeiro, J.A. Queiroz, G.A. Monteiro, P. Perrin, N. Tordo, D.M. F. Prazeres, Scale-up of hydrophobic interaction chromatography for the purification of a DNA vaccine against rabies, Biotechnol. Letts. 22 (2000) 1397–1400.
[30] M.M. Diogo, J.A. Queiroz, D.M.F. Prazeres, Studies on the retention of plasmid DNA and Escherichia coli nucleic acids by hydrophobic interaction chromatography, Bioseparation 10 (2001) 211–220.
[31] M.A. Esquibel-King, A.C. Dias-Cabral, J.A. Queiroz, N.G. Pinto, Study of hydrophobic interaction adsorption of bovine serum albumin under overloaded conditions using flow microcalorimetry, J. Chromatogr. A 865 (1999) 111–122.
[32] H. Li, Y. Yang, Y. Zhang, S. Zhang, Q. Zhao, Y. Zhu, X. Zou, M. Yu, G. Ma, Z. Su, A hydrophobic interaction chromatography strategy for purification of inactivated foot-and-mouth disease virus, Protein Expr. Purif. 113 (2015) 23–29.
[33] T. Weigel, R. Soliman, M.W. Wolff, U. Reichl, Hydrophobic-interaction chromatography for purification of influenza A and B virus, J. Chromatogr. B. 1117 (2019) 103–117.

[34] C.C. Shepard, A. Tiselius, The chromatography of proteins. The effect of salt concentration and pH on the adsorption of proteins to silica gel, Discuss. Faraday Soc. 7 (1949) 275–285.
[35] W.R. Melander, C. Horváth, Salt effects on hydrophobic interactions in precipitation and chromatography of proteins: an interpretation of the lyotropic series, Arch. Biochem. Biophys. 183 (1977) 200–215.
[36] W.R. Melander, D. Corradini, C. Horváth, Salt-mediated retention of proteins in hydrophobic-interaction chromatography: application of solvophobic theory, J. Chromatogr. A 317 (1984) 67–85.
[37] D. Nagrath, F. Xia, S.M. Cramer, Characterization and modeling of nonlinear hydrophobic interaction chromatographic systems, J. Chromatogr. A 1218 (2011) 1219–1226.
[38] P. Gagnon, Use of hydrophobic interaction chromatography with a non-salt buffer system for improving process economics in purification of monoclonal antibodies, in: Waterside Conference on Monoclonal and Recombinant Antibodies Miami, FL, USA, April 30 – May 3, 2000.
[39] A.W. Bamforth, Corrosion problems of ammonium sulphate manufacture, Anti-Corros. Method. M. 1 (1954) 31–35.
[40] S. Ghose, Y. Tao, L. Conley, D. Cecchini, Purification of monoclonal antibodies by hydrophobic interaction chromatography under no-salt conditions, MAbs 5 (2013) 795–800.
[41] P. Gagnon, Polishing methods for monoclonal IgG purification, in: AA Shukla, MR Etzel, S Gadam (Eds.), Process Scale Bioseparations for the Biopharmaceutical Industry, Taylor & Francis, New York:, 2006, pp. 491–505.
[42] T. Arakawa, S.N. Timasheff, Preferential interactions of proteins with solvent components in aqueous amino acid solutions, Arch. Biochem. Biophys. 224 (1983) 169–177.
[43] A.T. Dilks, J. Gilchrist, Y. Lam, N. Nicholes, B. Stanley, Considerations for operational space definition and optimization of a no-salt flowthrough hydrophobic interaction chromatography purification step, Biotechnol. Prog. 39 (2023) e3351.
[44] J. Chen, J. Tetrault, A. Ley, Comparison of standard and new generation hydrophobic interaction chromatography resins in the monoclonal antibody purification process, J. Chromatogr. A 1177 (2008) 272–281.
[45] T.K.H. Müller, M. Franzreb, Suitability of commercial hydrophobic interaction sorbents for temperature-controlled protein liquid chromatography under low salt conditions, J. Chromatogr. A 1260 (2012) 88–96.
[46] S. Hjertén, J. Rosengren, P. Sven, Hydrophobic interaction chromatography: the synthesis and the use of some alkyl and aryl derivatives of agarose, J. Chromatogr. A 101 (1974) 281–288.
[47] X. Geng, L. Guo, J. Chang, Study of the retention mechanism of proteins in hydrophobic interaction chromatography, J. Chromatogr. A 507 (1990) 1–23.
[48] Z. El Rassi, Recent progress in reversed-phase and hydrophobic interaction chromatography of carbohydrate species, J. Chromatogr. A 720 (1996) 93–118.
[49] D. Haidacher, A. Vailaya, C. Horváth, Temperature effects in hydrophobic interaction chromatography, Proc. Natl. Acad. Sci. 93 (1996) 2290–2295.
[50] R. Muca, W. Piątkowski, D. Antos, Effects of thermal heterogeneity in hydrophobic interaction chromatography, J. Chromatogr. A 1216 (2009) 6716–6727.
[51] R. Muca, W. Piątkowski, D. Antos, Altering efficiency of hydrophobic interaction chromatography by combined salt and temperature effects, J. Chromatogr. A 1216 (2009) 8712–8721.
[52] R. Muca, W. Marek, W. Piątkowski, D. Antos, Influence of the sample-solvent on protein retention, mass transfer and unfolding kinetics in hydrophobic interaction chromatography, J. Chromatogr. A 1217 (2010) 2812–2820.
[53] P. Cao, T.K.H. Müller, B. Ketterer, S. Ewert, E. Theodosiou, O.R.T. Thomas, M. Franzreb, Integrated system for temperature-controlled fast protein liquid chromatography. II. Optimized adsorbents and 'single column continuous operation, J. Chromatogr. A 1403 (2015) 118–131.
[54] J.E. Berlier, A. Rothe, G. Buller, J. Bradford, D.R. Gray, B.J. Filanoski, W. G. Telford, S. Yue, J. Liu, C.Y. Cheung, W. Chang, Quantitative comparison of long-wavelength Alexa Fluor dyes to Cy dyes: fluorescence of the dyes and their bioconjugates, J. Histochem. Cytochem. 51 (2003) 1699–1712.
[55] J.J. Stickel, A. Fotopoulos, Pressure-flow relationships for packed beds of compressible chromatography media at laboratory and production scale, Biotechnol. Prog. 17 (2001) 744–751.
[56] J. Schindelin, I. Arganda-Carreras, E. Frise, V. Kaynig, M. Longair, T. Pietzsch, S. Preibisch, C. Rueden, Saalfeld S, B. Schmid, J.-Y. Tinevez, D.J. White, V. Hartenstein, K. Eliceiri, P. Tomancak, A. Cardona, Fiji: an open-source platform for biological-image analysis, Nat. Methods. 9 (2012) 676–682.
[57] F. Crameri, G.E. Shephard, P.J. Heron, The misuse of colour in science communication, Nat. Commun. 11 (2020) 5444.
[58] H.P. Jennissen, L.M.G. Heilmeyer Jr, General aspects of hydrophobic chromatography. Adsorption and elution characteristics of some skeletal muscle enzymes, Biochemistry 14 (1975) 754–760.
[59] B.H.J. Hofstee, N.F. Otillio, Non-ionic adsorption chromatography of proteins, J. Chromatogr. A 159 (1978) 57–69.
[60] W.Y. Chen, H.M. Huang, C.C. Lin, F.Y. Lin, Y.C. Chan, Effect of temperature on hydrophobic interaction between proteins and hydrophobic adsorbents: studies by isothermal titration calorimetry and the van't Hoff equation, Langmuir 19 (2003) 9395–9403.
[61] A. Susanto, T. Herrmann, E. von Lieres, J. Hubbuch, Investigation of pore diffusion hindrance of monoclonal antibody in hydrophobic interaction chromatography using confocal laser scanning microscopy, J. Chromatogr A. 1149 (2007) 178–188.
[62] J.A. Roberts, L. Kimerer, G. Carta, Effects of molecule size and resin structure on protein adsorption on multimodal anion exchange chromatography media, J. Chromatogr. A 1628 (2020) 461444.
[63] R. Ueberbacher, A. Rodler, R. Hahn, A. Jungbauer, Hydrophobic interaction chromatography of proteins: thermodynamic analysis of conformational changes, J. Chromatogr. A 1217 (2010) 184–190.
[64] A. Jungbauer, C. Machold, R. Hahn, Hydrophobic interaction chromatography of proteins: III. Unfolding of proteins upon adsorption, J. Chromatogr. A 1079 (2005) 221–228.
[65] P.P. Madeira, I.L. Rocha, M.E. Rosa, M.G. Freire, J.A. Coutinho, On the aggregation of bovine serum albumin, J. Mol. Liq. 349 (2022) 118183.
[66] J.A. Roberts, G. Carta, Protein adsorption and separation with monomodal and multimodal anion exchange chromatography resins. Part II. Mechanisms of protein aggregation on the chromatographic surface, J. Chem. Technol. Biotechnol. 98 (2023) 357–368.
[67] C. Honda, H. Kamizono, T. Samejima, K. Endo, Studies on thermal aggregation of bovine serum albumin as a drug carrier, Chem. Pharm. Bull. 48 (2000) 464–466.
[68] V.A. Borzova, K.A. Markossian, N.A. Chebotareva, S.Y. Kleymenov, N.B. Poliansky, K.O. Muranov, V.A. Stein-Margolina, V.V. Shubin, D.I. Markov, B.I. Kurganov, Kinetics of thermal denaturation and aggregation of bovine serum albumin, PLoS ONE 11 (2016) e0153495.
[69] M.A. Mata-Gómez, S. Yaman, J.A. Valencia-Gallegos, C. Tari, M. Rito-Palomares, J. González-Valdez, Synthesis of adsorbents with dendronic structures for protein hydrophobic interaction chromatography, J. Chromatogr. A 1443 (2016) 191–200.
[70] S. Tan, K. Saito, M.T. Hearn, Stimuli-responsive polymeric materials for separation of biomolecules, Curr. Opin. Biotechnol. 53 (2018) 209–223.
[71] S. Tan, E.M. Campi, R.I. Boysen, K. Saito, M.T. Hearn, Batch binding studies with thermo-responsive polymer grafted Sepharose 6 Fast Flow sorbents under different temperature and protein loading conditions, J. Chromatogr. A 1625 (2020) 461298.
[72] J.P. Gabrielson, M.L. Brader, A.H. Pekar, K.B. Mathis, G. Winter, J.F. Carpenter, T. W. Randolf, Quantitation of aggregate levels in a recombinant humanized monoclonal antibody formulation by size-exclusion chromatography, asymmetrical flow field flow fractionation, and sedimentation velocity, J. Pharm. Sci. 96 (2007) 268–279.
[73] M. Vazquez-Rey, D.A. Lang, Aggregates in monoclonal antibody manufacturing processes, Biotechnol. Bioeng. (2011) 1494–1508.
[74] E.M. Moussa, J.P. Panchal, B.S. Moorthy, J.S. Blum, M.K. Joubert, L.O. Narhi, E. M. Topp, Immunogenicity of therapeutic protein aggregates, J. Pharm. Sci. 105 (2016) 417–430.
[75] A. Michnik, Thermal stability of bovine serum albumin DSC study, J. Therm. Anal. Calorim. 71 (2002) 509–519.
[76] M.L. Brader, T. Estey, S. Bai, R.W. Alston, K.K. Lucas, S. Lantz, P. Landsman, K. M. Maloney, Examination of thermal unfolding and aggregation profiles of a series of developable therapeutic monoclonal antibodies, Molec. Pharm. 12 (2015) 1005–1017.
[77] N. Kohli, N. Jain, M.L. Geddie, M. Razlog, L. Xu, A.A. Lugovskoy, A novel screening method to assess developability of antibody-like molecules, MAbs 7 (2015) 752–758.
[78] D. Molodenskiy, E. Shirshin, T. Tikhonova, A. Gruzinov, G. Peters, F. Spinozzi, Thermally induced conformational changes and protein–protein interactions of bovine serum albumin in aqueous solution under different pH and ionic strengths as revealed by SAXS measurements, Phys. Chem. Chem. Phys. 19 (2017) 17143–17155.
[79] P. Garidel, A. Eiperle, M. Blech, J. Seelig, Thermal and chemical unfolding of a monoclonal IgG1 antibody: application of the multistate Zimm-Bragg theory, Biophys. J. 118 (2020) 1067–1075.
[80] F. Sert, D. Hız, M. Gülmez, S.E. Cankurtaran, C.I. Kayalan, H. Kurt, M. Yüce, Temperature and pH-dependent behaviors of mAb drugs: a case study for trastuzumab, Sci. Pharm. 90 (2022) 21.